CHAPTER 2

Effect of Novel PCM Encapsulation Designs on Electrical and Thermal Performance of a Hybrid Photovoltaic Solar Panel

Encapsulated phase change materials (PCM) are used to improve the electrical efficiency of photovoltaic (PV) panel by absorbing waste heat during the melting process. Previous investigators reported the melting process of PCM in a rectangular encapsulation and observed four transient regimes of heat transfer in sequence as: conduction, mixed conduction-convection, quasi-steady convection and solid-shrinking regimes. For higher heat extraction from the PV panel, longer duration of quasi-steady convection regime is desirable. However, this steady regime is suppressed in the rectangular PCM enclosure due to the nature of natural convection and consequently, the melting rate of the PCM is arrested. In this chapter, we report on electrical and thermal performance of non-rectangular PCM integrated PV panels using an experimentally validated numerical model that enhances the quasi-steady regime by more than 100% compared to the conventional rectangular design. The strategic mass distribution of PCM for better thermal management was achieved with encapsulation designs having profile of right wall varying as $y = (ax - b)^{(1/n)}$*,with n=1 (linear),2 (parabolic) and 3 (cubic) with different lower thickness ratio. Compared to conventional design, the proposed design increased the PCM melting rate by 17% due to which PV cell temperature dropped by 11.5% and consequently, electrical conversion efficiency approaches to 12%.*

2.1 Introduction

The global energy demand has been continuously increasing with the growth in population and progress in technology during last few decades. With this increase in energy demand, its pri-

mary source like fossil fuels are being used in excess and are on the verge of extinction. Use of fossil fuels also leads to pollution and global warming. These problems can be minimized with the increase in use of solar energy like photovoltaics (PV) technology in future. PV converts solar energy into electrical energy. However, one major disadvantage of this technology is that all of incoming radiation is not converted into electricity, and most of it i.e. more than 80% is wasted as heat energy which increases the temperature of PV cell. Electrical performance of PV cell is affected by its operating temperature. PV cell efficiency shows a drop of 0.65% per degree rise of temperature [40]. If efficiency of PV panel has to be increased then this heat must be extracted from the panel. Such photovoltaic thermal collector system (PV/T) has gained special attention by the research community in recent times [9, 41, 42]. Many researchers have done experimental and theoretical studies on PV/T systems which are generally classified as air cooled PV/T systems [10, 43, 44] water cooled PV/T systems [45–47] and PCM cooled PV/T systems [6, 34, 48]. Some of the configurations of PV/T system uses more than one fluid such as air-water cooled, and air-PCM and water-PCM cooled PV/T systems [34, 48, 49]. Use of such configurations enhances the performance of PV systems but they still have some disadvantages. Some of the drawbacks of air cooled PV/systems are that air has very low specific heat and hence, the amount of heat that can be extracted is limited. Further heat transfer rate can be increased by increasing air flow rates using pump, however, it increases the electrical energy input in overcoming the high pressure drop. The problem of low specific heat can be removed by replacing air by a high specific heat fluid such as water. Water can absorb about four time as much as heat as air. However, water has high density and hence requires a considerable pumping power. Furthermore, water and air can't store heat for off-sunshine hours. Phase change materials (PCM) has great potential for storing heat and using the latent heat energy when required in off-sunshine hours or during night. They have high latent heat with almost constant phase change temperature. This relatively constant phase change temperature gives an almost constant operating temperature when attached to PV system.

When PCM encapsulation is attached at the back of a PV panel, the design of encapsulation is mainly follows the design of PV panel. Since the PV panel designs are mostly thin rectangular sheets, PCM encapsulation follows the same design (see Figure 2.1 (a)). This is reason that most of the previous investigators have used a conventional rectangular design of PCM encapsulation (see Table 2.1) integrated with the PV panel to extract heat under natural convection condition. Various methods have been used to augment the heat transfer and hence, PV electrical efficiency (mentioned in Table 2.1), however, the effect of PCM enclosure design has been altogether overlooked. It is also clear from the Table 2.1 that electrical efficiency increases with the use of PCM albeit it varies depending on the system configurations. In order to design an efficient PCM enclosure it is important to understand the melting process under the effect of natural convection.

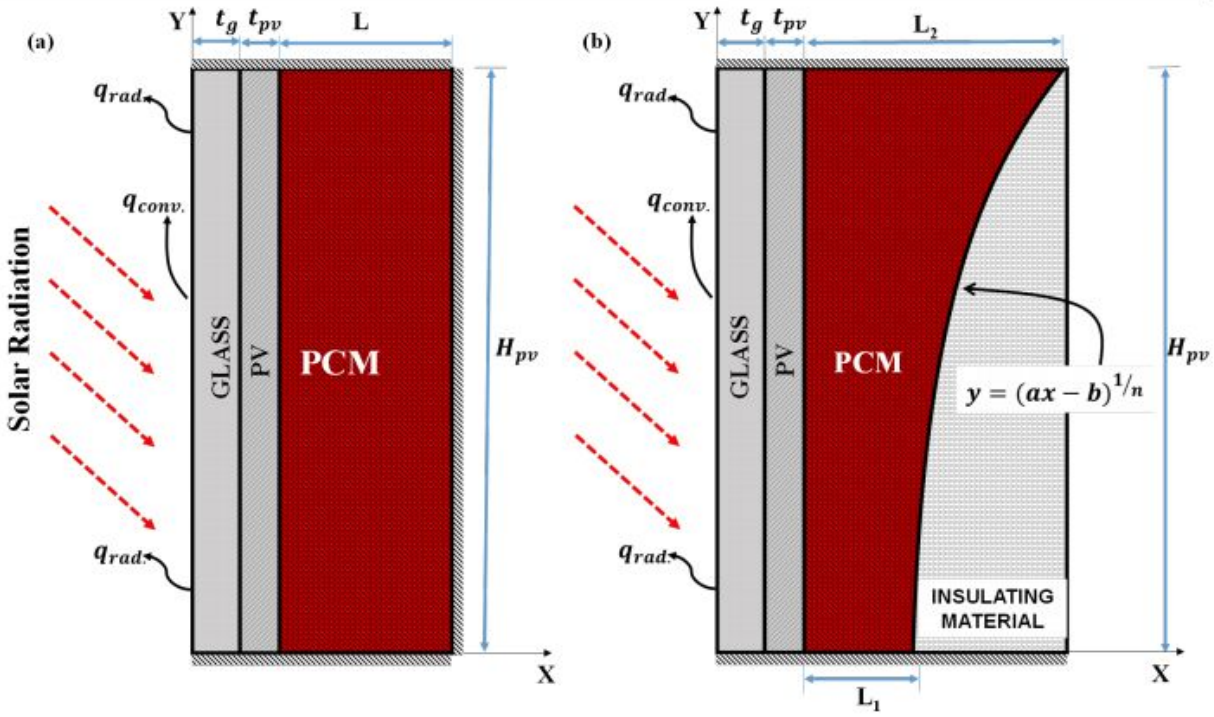

Figure 2.1: Schematic diagram showing cross-section of PV/PCM system with (a) type-A conventional rectangular PCM enclosure, (b) type-B, C, & D non-rectangular PCM enclosure with a general profile, $y = (ax-b)^{(1/n)}$, n=1 for type-B, n=2 for type-C and n=3 for type-D.

Table 2.1: Relevant literature on PCM integrated with PV module. Note that only rectangular type encapsulation design has been reported.

Authors	**Type of Encapsulation**	**Type of System**	**Findings**
Hasan et al., [6]	Rectangular	PV/PCM	• PCM C-P and $CaCl_2$ – Temperature reduction: 18°C. • $CaCl_2$– Temperature reduction: 10°C (duration: 5 hours, insolation: 1000 W/m^2).
Yang et al., [48]	Rectangular	PV/T PV/T-PCM	• Maximum temperature reduction: 15.8°C. • η_{pv}– PV/T: 6.98%, PV/T-PCM: 8.16%. • $\eta_{thermal}$– PV/T: 58.35%, PV/T-PCM: 70.34%. • Primary energy saving efficiency: 14%.
Su et al., [34]	Rectangular	Air PV/T-PCM	• Preferable configuration: Upper PCM mode • η_{pv}increment: 10.7%. •Optimum PCM thickness: 3 cm.

Ho et al., [49]	Rectangular	PV integrated with water saturated MEPCM layer	• Optimum PCM thickness: 5 cm (Melting Temperature: 30°C). • The highest temperature reduction: 1.8°C • Power output increment: 2.1%.
Ezan et al., [36]	Rectangular	BIPV/PCM	• Increased PCM thickness – Melting rate: convection model > conduction model. • PCM thickness (10 cm) – PV temperature: convection (50%) < conduction.
Lu et al. [50]	Rectangular	Concentrating BIPV/PCM	• Only PCM – η_{pv}: 10% , Temperature reduction : 20°C. • Thermoelectric performance: Vertical fins > horizontal fins. • Vertical fins – Temperature drop: 25°C.
Khanna et al., [51]	Rectangular	Finned PV/PCM	• Finned PCM – Most suitable depth: 2.8 cm (global radiation: 3 $kWh/m^2/day$), 4.6 cm (global radiation: 5 $kWh/m^2/day$). • Without fins – Most suitable depth: 2.3 cm (global radiation: 3 $kWh/m^2/day$), 3.9 cm (global radiation: 5 $kWh/m^2/day$).
Kibria et al., [52]	Rectangular	PV/PCM	• Lowest PV temperature – RT28HC (high latent heat). • η_{pv}increment: 5%.
Huang et al. [53]	Rectangular	BIPV/PCM	• Significant improvement in electrical performance with PCM.
Nasef et al., [54]	Rectangular	Nano-fluid and PCM integrated PV	• Power output increment: 2.5%. • Melting time decrement: 12%.
Rabie et al., [55]	Rectangular	Concentrating PV/PCM	• Inclination angle (-45°), concentration ratio (5) and over-height ratio (0-60%) – Peak cell temperature: 92°C–74°C and temperature uniformty: 13.7-5.3°C.
Emam and Ahmed, [56]	Rectangular	Concentrating PV/PCM	• Single cavity (concentration ratio 20) – CPV cell temperature < 124°C. • Five parallel cavity – CPV temperature: 72°C and η_{pv}: 17.7%.

Hassan et al., [57]	Rectangular	Nano-fluids integrated PV/T-PCM	• PV/T-PCM (nano-fluids) – η_{pv} enhancement: 23.9%. • PV/T-PCM (water) – η_{pv} enhancement: 22.7%. • PV/PCM – η_{pv} enhancement: 9.1%.
Nada et al., [58]	Rectangular	PV integrated with nano-PCM	• PV/nano-PCM – η_{pv} enhancement: 13.2%. • PV/nano-PCM temperature reduction: 10.6°C. • PV/PCM – η_{pv} enhancement: 22.7%. • PV/PCM temperature reduction: 8.1°C.
Li et al., [59]	Rectangular	PV/T PV/T-PCM	• Temperature reduction: 23°C. • η_{pv}enhancement: 5.18%.
Al-Waeli et al., [60]	Rectangular	Nano-fluid based PV/nano-PCM	• Temperature reduction: 30°C. • η_{pv}enhancement: 7.1% – 13.75%.

The melting process is generally categorized in four different regimes (Jany and Bejan, [38]) in a rectangular enclosure. (i) Conduction regime, in which the melting takes place only due to conduction heat transfer, (ii) mixed regime, in which the heat transfer to PCM occurs by both conduction and convection. As time progresses, heat transfer by conduction starts to diminish and onset of convection mode starts to prevail, (iii) the quasi-steady convection regime; in which heat transfer is totally dominated by convection currents and the system nearly reach a steady state mode. This regime ends when melting front reaches right wall, and (iv) solid shrinking regime; in this regime, melting slows down due to suppression of convection current. Recently, Kamkari et al. [37] conducted a study on the effect of inclination angle on convection driven melting of PCM in a rectangular enclosure. They reported that melting becomes slower in rectangular enclosure due to suppression of convection current. They also concluded that heat transfer by natural convection increases with inclination angle when PCM enclosure is heated from the bottom side and maximum melting is observed in horizontal enclosure.

Two critical observations from the above discussion is made (i) melting slows down in rectangular enclosure in later stages of melting due to suppression of convection current in solid shrinking regime and (ii) a symmetric enclosure for PCM encapsulation like the rectangular design is not a suitable attachment to the PV panel. It is an established fact that melting process, specifically during the convection regime, is not symmetric [37, 38] then why the design encapsulating the PCM be symmetric? With strategic distribution of PCM in the enclosure, duration

of solid shrinking regime can be decreased and hence, dominance of quasi-steady convection regime can be enhanced. Heat transfer by natural convection dominates in the top region of enclosure. Further Akgun et al., [61] and Seddegh et al., [62] confirmed that conical (unsymmetrical) latent heat thermal energy storage (LHTES) cavity can store thermal energy faster than cylindrical (symmetrical) LHTES cavity due to enhancement in natural convection. Clearly, the conventional rectangular PCM enclosure design does not aid in natural convection and detailed investigation of PV/PCM system with unsymmetrical PCM enclosure is rarely reported. In this study we report the investigation on enclosure design of PCM that aid in natural convection and consequently, increases melting rate and heat transfer coefficient. The main objective of this study is to extend the quasi-steady convection regime of melting at the expense of last regime i.e. the solid shrinking regime by the strategic distribution of same volume of PCM. To achieve the stated objective, new enclosure designs are conceived as demonstrated in Figure 2.1(b). The linear wall (opposite to PV module) is developed into non-rectangular generic shapes with profile varying as power of *1/n*. For $n = 2$ and 3, the profile becomes parabolic and cubic respectively. Though there can be numerous such profiles that can be studied, the investigated shapes can be used as guidance for further research and development of efficient enclosure designs. These three different configurations of PCM enclosure integrated with a building integrated PV (BIPV) system has been studied under same boundary conditions. The experimentally validated numerical modelling of PV/PCM system has been carried out to investigate the influence of natural convection on improved design compare to conventional rectangular one. In this paper, it has been found that the change of shape of enclosure influences the natural convection with in liquid PCM significantly. Data and design investigation presented in this paper would assist the research community in designing a better enclosure shapes that would further enhance the thermal and electrical performance of a PV/T module.

2.2 Material & method

2.2.1 Problem description & definition

Two-dimensional mathematical model of PV/PCM system was created (see Figure 2.1) for investigating the thermal performance of PV panel when different types of PCM cavities are attached to it. PV panel comprises a glass layer ($t_g = 3mm$) and PV cell ($t_{pv} = 1mm$) and the height of the computational domain (H) is 100 mm. The computational domain consists of four different geometrical configurations of PCM enclosure attached to the rear side of PV system. A conventional rectangular PCM enclosure of thickness 20 mm is attached to PV panel in type-A configuration. In type-B, C, & D configuration, rectangular enclosure is replaced by non-rectangular enclosure. The right-most wall of non-rectangular enclosure has a general profile of $y = (ax - b)^{(1/n)}$, which is different in all configurations. For type-B, the profile is linear ($n = 1$),

for type-C the profile is parabolic ($n = 2$) and for type-D the profile is cubic ($n = 3$). Here the constant "a" and "b" are adjusted in such a way that the volume of PCM for all investigated configuration is same as in the rectangular enclosure. Rubitherm RT27 is used as PCM in all different type of enclosures and thermo-physical properties of RT27 has been listed in Table 2.2 [36]. The PCM properties are same for both solid and liquid phases, all thermo-physical properties of PCM are independent of temperature except density which varies with temperature according to Boussinesq approximation.

Solar radiation (I_{solar}) is incident on the left wall, and at the same time, there are convective ($q^{"}_{conv}$) and radiative heat flux losses($q^{"}_{rad}$) from the left wall i.e on the outer surface of glass.

$$[-k\frac{dT}{dx}]_{x=0} = I_{solar} - q^{"}_{conv} - q^{"}_{rad} \tag{2.1}$$

Convective heat transfer takes place from the surface to surroundings by both forced and natural convection.

$$q^{"}_{conv} = h_t(T_s - T_a) \tag{2.2}$$

whereT_s and T_a denote the temperature of exterior surface and ambient/surrounding, respectively. The term convection heat transfer coefficient i.e.h_t denote cumulative heat transfer accompanied between exterior surface and ambient condition. Hendricks and Sark [63] propose the cumulative convection heat transfer coefficient given as,

$$h_t = (h_n^3 + h_w^3)^{(1/3)} \tag{2.3}$$

The natural heat transfer coefficient(h_n) and forced heat transfer coefficient (h_w) using equations proposed by Hendricks and Sark [63],

$$h_n = 1.78(T_s + T_a)^{(1/3)} \tag{2.4}$$

$$h_w = 2.8 + 3.0v_w \tag{2.5}$$

In Eq. 2.4, the values of temperatures of ambient (T_a) and surface (T_s) were taken in kelvin (K). In Eq.2.5, on the other hand, wind speed (v_w) is measured in m/s.

The radiation heat loss between outer space/sky and exterior surface can be calculated by Stefan-Boltzmann equation for radiative heat transfer,

$$q^{"}_{rad} = \varepsilon\sigma(T_s^4 - T_{sky}^4) \tag{2.6}$$

where ε is the emissivity of the surface, σ is the Boltzmann constant and T_{sky} is the temperature of open sky. The right, bottom and top surfaces of considered geometry have been assumed perfectly insulated.

Table 2.2: Thermo-physical properties of materials .

Materials	Specific heat (J/kgK)	Density (kg/m^3)	Thermal conductivity (W/mK)	Latent heat of fusion (J/kg)	Dynamic viscosity (kg/ms)	Thermal expansion coeff. (1/K)	Melting temperature (°C)
Glass	500	3000	1.8	-	-	-	-
PV cell	1255	1760	0.1	-	-	-	-
PCM	2000	880	0.2	184000	0.0044	0.00091	27

Table 2.3: Design specifications and boundary conditions for all geometric configurations.

Case	Type	Enclosure	Exponent (n) of right wall profile	Lower thickness ratio $\left(\frac{L_1}{L}\right)$	Bifurcation mass ratio $\left(\frac{m_{upper}}{m_{lower}}\right)$
	A	Rectangular	-	1	1
Case 1	B	Non-Rectangular	1	0.1	2.63
	C	Non-Rectangular	2	0.1	5.15
	D	Non-Rectangular	3	0.1	8.41
Case 2	B	Non-Rectangular	1	0.3	2.07
	C	Non-Rectangular	2	0.3	3.21
	D	Non-Rectangular	3	0.3	4.16
Case 3	B	Non-Rectangular	1	0.5	1.67
	C	Non-Rectangular	2	0.5	2.2
	D	Non-Rectangular	3	0.5	2.55

For all type of geometric configurations:

At $y = 0 \rightarrow [\frac{dT}{dy}]_{(y=0)} = 0$, $y = H \rightarrow [\frac{dT}{dy}]_{(y=H)} = 0$,

For type-A:

At $x = L + t_g + t_{pv} \rightarrow [\frac{dT}{dx}]_{(x=L+t_g+t_{pv})} = 0$,

For type-B, C & D:

Along the curvature of right wall, $\frac{dT}{dx} = 0$.

In the present analysis various numerical simulations are conducted with constant boundary conditions and a comparative study between all geometric configurations is conducted for different cases. Three different cases of study has been formed on the basis of lower thickness

ratio (ratio of lower thickness of PCM in non-rectangular enclosure to thickness of PCM in rectangular enclosure, $\frac{L_1}{L}$). L_1 is kept constant for each profile while L_2 is variable in order to kept same volume of PCM for a given case. All three cases with different geometric configuration and boundary conditions are listed in Table 2.3.

In case 1 PV/PCM system with all three non-rectangular PCM enclosure is being studied at $\frac{L_1}{L} = 0.1$, while $\frac{L_1}{L} = 0.3$, and 0.5 for case 2 and case 3 respectively. These values are calculated based on thermal diffusion length. Different values of $\frac{L_1}{L}$ is selected to investigate the effect of width of bottom side of the enclosure. A higher value of thickness ratio suggests higher volume of PCM in the lower part of enclosure. Each case at different configuration exhibit different bifurcation mass ratio $\frac{m_{upper}}{m_{lower}}$ (ratio of mass of PCM in upper half to lower half of enclosure on the basis of height of PV panel, $\frac{H}{2}$ each half). Bifurcation mass ratio depicts the distribution of mass in enclosure. A higher value of bifurcation mass ratio suggests higher mass of PCM in the upper part of enclosure. The solar insolation (I_{solar}), wind velocity (v_w) and the ambient temperature (T_a) were considered constant in the numerical analysis.

2.2.2 Solution method

The computational domain is divided into three components, which are glass, PV cell and PCM. In glass and PV cell layer heat transfer takes place through conduction only, while in PCM enclosure heat transfer is dominated by conduction as well as convection simultaneously. Following assumptions have been considered are: (a) liquid PCM as an incompressible and Newtonian fluid, (b) no viscous heating, (c) flow considered as laminar, (d) PCM is pure with same solidus and liquid temperature and (e) Boussinesq approximation (density is considered constant, except in the gravity forces term).

The conservations equations are given as follows:

Mass conservation equation:

$$\frac{\partial \rho}{\partial t} + \nabla . (\rho \vec{u}) = 0 \tag{2.7}$$

Momentum conservation equation:

$$\frac{\partial (\rho \vec{u})}{\partial t} + (\rho \vec{u} . \nabla) \vec{u} = \nabla . (\mu \nabla \vec{u}) - \nabla P + S_{Darcy} + S_{Boussinesq} \tag{2.8}$$

Where

$$S_{Darcy} = -\frac{B_{mush}(1-f_l)^2}{(f_l^3+\epsilon)} \vec{u}, S_{Boussinesq} = \rho \vec{g} \beta (T - T_m) \tag{2.9}$$

The constant B_{mush} in the Darcy term governs the transition at solid-liquid interface. However, higher value of $B_{mush}(10^9)$ based on suggestions by Soni et al. [64] is considered for present study in order to achieve steeper change of flow velocity at the time of phase change. At very ini-

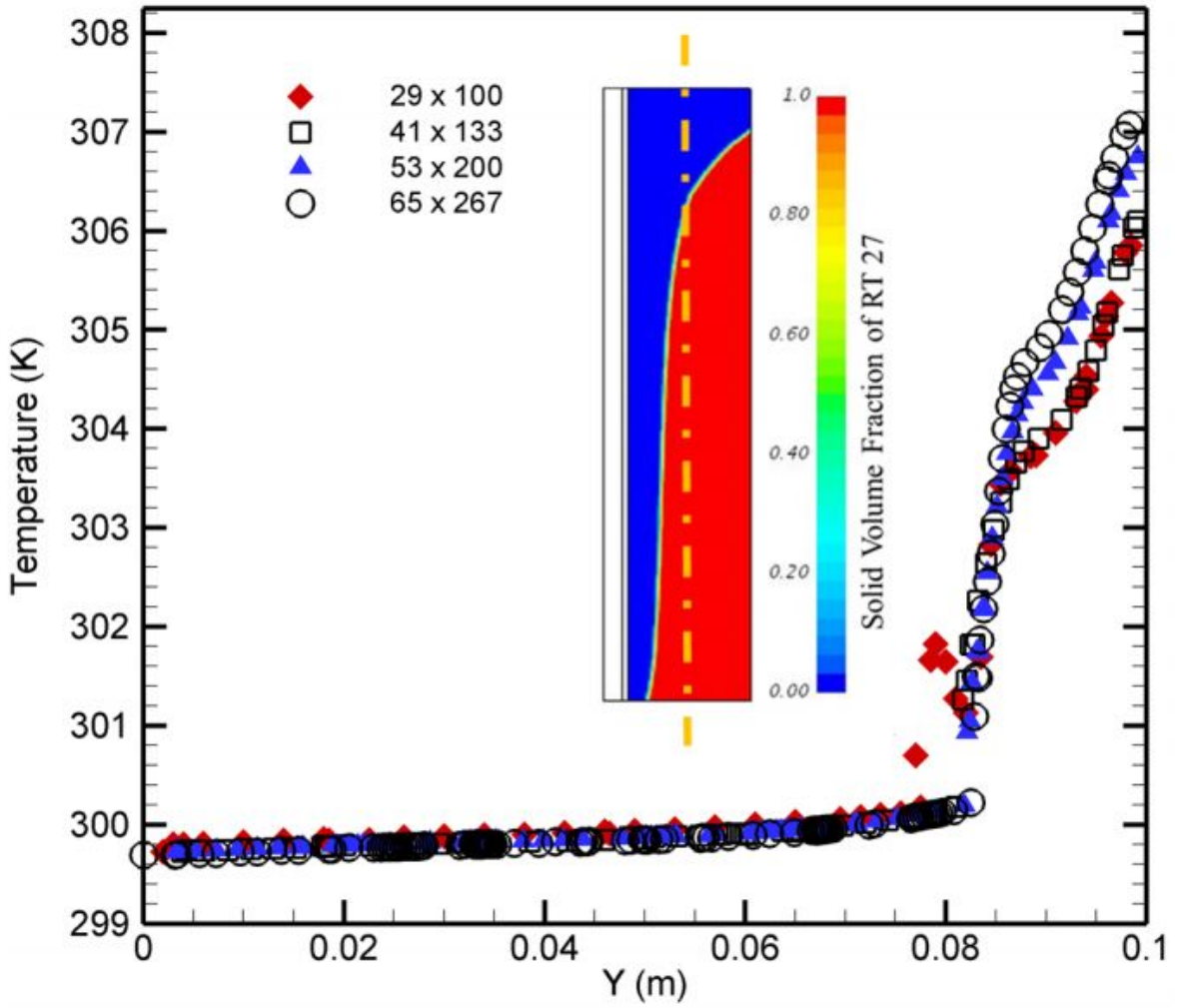

Figure 2.2: Variation of centerline temperature at 3600 s for different number of grids. Inset shows the melting front of PCM. Location of centerline is marked in the figure by dash-dot line.

tial, the liquid fraction f_l is zero, and hence a very small constant value ϵ (0.0001) is added to the denominator of the Darcy term to avoid divergence. In Eq. 2.8 the Boussinesq term is added on the right side to consider buoyancy effect generated due to gravity.

Energy conservation equation:

The energy conservation equation with the assumption of same thermos-physical properties of solid-liquid phase can be written as:

$$\frac{\partial(\rho c_p T)}{\partial t} + \nabla.(\rho c_p \vec{u} T) = \nabla.(k\nabla T) + \frac{\partial(\rho f_l L_{sf})}{\partial t} \tag{2.10}$$

The second term on the right hand side of Eq. 2.10 represents the heat absorption or generation during melting or solidification phase change. The energy equation for PV and glass layers is written as follows:

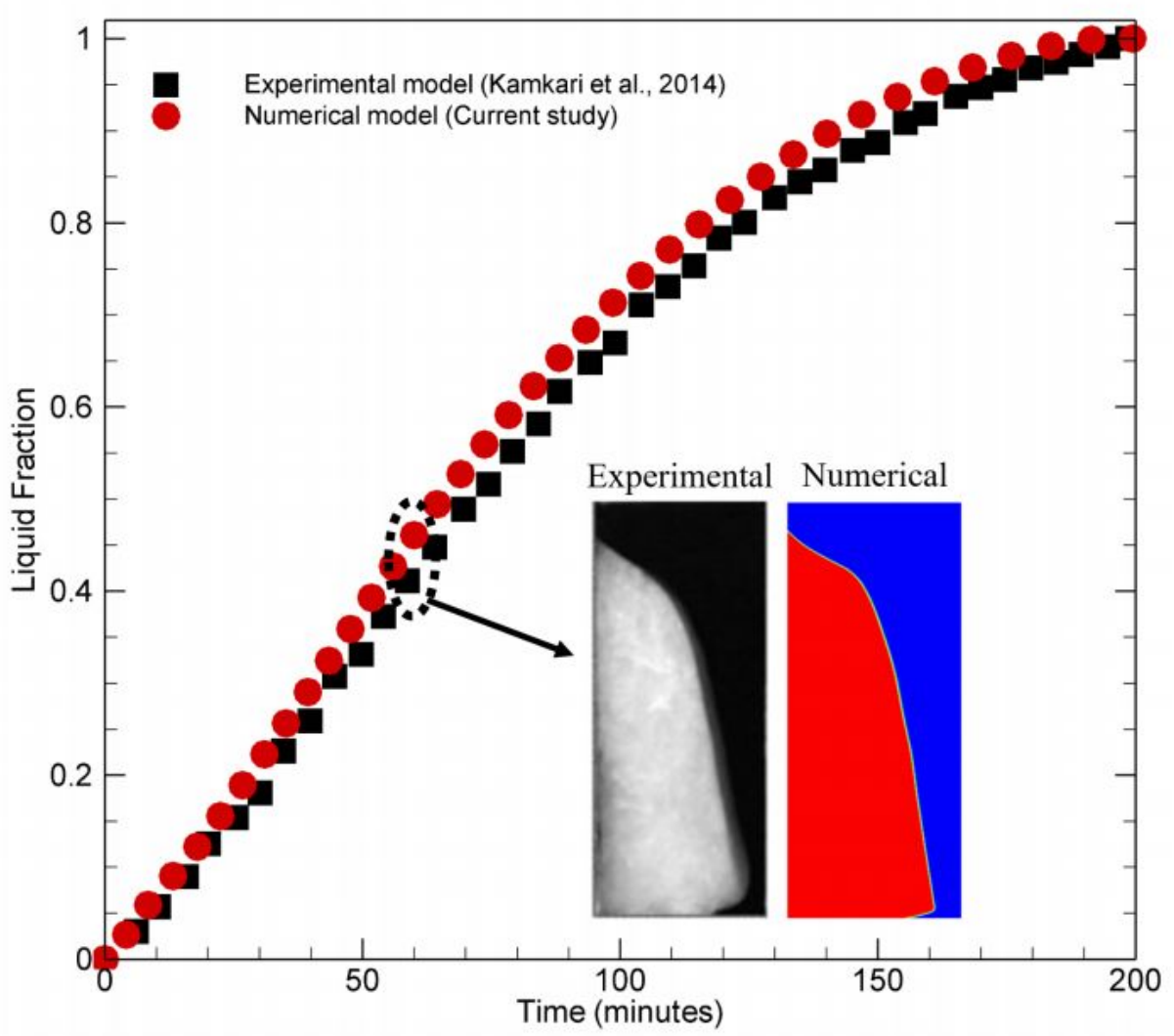

Figure 2.3: Variation of liquid fraction of PCM predicted from numerical model and experimental study (Kamkari et. al 2014). Two figures in the inset shows the instantaneous liquid fraction: left [experimental] and right [numerical].

$$\frac{\partial(\rho c_p T)}{\partial t} = \nabla \cdot (k \nabla T) - P'''_{out.} + Q'''_{gen.} \tag{2.11}$$

On the right-hand side of Eq. 2.11, the term $P'''_{out.}$ denote the volumetric power generation for PV layers while $Q'''_{gen.}$ is the energy source term due to solar radiation absorb by PV cells.

$$P'''_{out.} = (\eta_{pv} * (\alpha_{pv} \tau_g I_{solar}))/t_{pv} \tag{2.12}$$

$$Q'''_{gen.} = ((1-\eta_{pv}) * (\alpha_{pv} \tau_g I_{solar}))/t_{pv} \tag{2.13}$$

where η_{pv} is the PV panel electrical conversion efficiency which depends on the temperature of the PV cell. The temperature dependency of electrical efficiency of PV cell is suggested by Evans and Flourschutez [65] by following equation:

$$\eta_{pv} = \eta_{ref}[1-\beta_{ref}(T_{pv}-T_{ref})] \tag{2.14}$$

In Eq. 2.14 electrical efficiency is calculated as the function of PV cell temperature corresponding to reference temperature $T_{ref} = 25°C$, $\beta_{ref} = 0.003921/K$ and $\eta_{ref} = 0.124$ [65]. The PV panel absorptivity (α_{pv}) and transmissivity of the glass (τ_g) were considered as 0.9 and 0.95 respectively [7].

2.2.3 Grid independence test

Conservation equations were solved for the discretized numerical domain using implicit stepping scheme. The velocity-pressure flow field have been resolved using SIMPLER algorithm. Algebraic finite volume coefficients are computed by using power law scheme in ANSYS-FLUENT solver. For unsteady simulation analysis time-step 0.05 s was considered. The convergence achieved based on the relative error of inner iterations and energy conservation.

The grid dependency test has been done by conducting the simulations with 29 x 100, 41 x 133, 53 x 200, and 65 x 267 grids for type – A enclosure. The centerline temperature along y-axis for PCM enclosure at 3600 s is shown in Figure 2.2. It is observed that there is relative error of 0.3% for the last two grid size. Based on the above grid independence test 53 x 200 grids was selected which undergone negligible variation with respect to finer grid size to save the simulation time duration and resources.

2.2.4 Validation with experimental eesults

For validation of the computational model, the experimental investigation of Kamkari et. al [37] on convection-driven melting of PCM in a rectangular enclosure is reproduced numerically. In this experimental work a rectangular cavity filled by PCM (lauric acid) was oriented at different inclination angles at 0, 45, and 90 degree. A constant temperature of 70°C, 60°C and 55°C was maintained at the right wall in three different experimental set up respectively and other three walls are kept insulated using different materials.

We have chosen the inclination angle of 90 degree and temperature of right wall at 70°C and a numerical study was conducted and compared with experimental results. The comparison of time evolution data from experimental and numerical solution is shown in Figure 2.3. It can be noticed from the figure that physical melting duration in the model takes a little earlier (196 minutes) than experimental solution (198.5 minutes). Also, during the melting a maximum error of 8.53% is found between the experimental and numerical data of liquid fraction. Figure

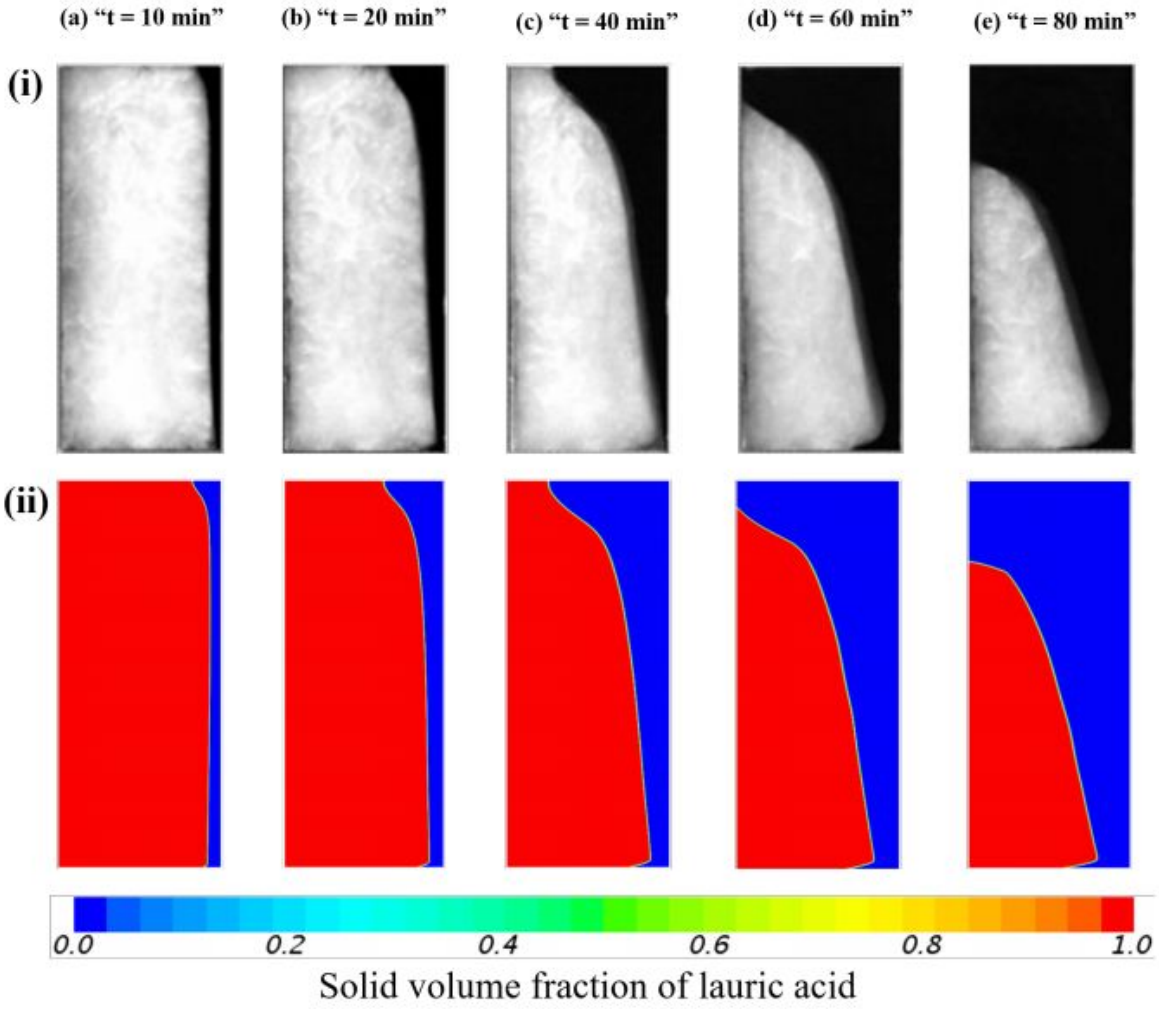

Figure 2.4: Solid-liquid interface patterns predicted from (i) experimental study by Kamkari et al., (2014) and (ii) numerical model.

2.4 demonstrate the comparison of position of solid-liquid interface from experimental and numerical studies. It has been found that numerical model shows similar melting patterns but exhibit marginally faster melting than the experimental model. Numerical model also exhibit lower melting rate in suppression regime as compare to experimental model causing a longer physical melting duration for it. This may be due to following reasons (i) assumption of PCM as pure substance in the model (ii) uncertainty in experimental measurements, and (iii) numerical error in the model. Considering these points, the errors in model prediction is reasonably close to the experimental data and hence, it can be assumed that the computational model mimics the experimental conditions.

2.3 Results and discussions

2.3.1 Solid-liquid interface patterns

Solid-liquid interface flow patterns provides a good visualization of the melting process and incumbent heat transfer mechanisms during phase change of the PCM. Figure 2.5, Figure 2.6, and Figure 2.7 show the sequential solid fraction contours of melting process for Case 1 (non-rectangular enclosure with $\frac{L_1}{L} = 0.1$), Case 2 (non-rectangular enclosure with $\frac{L_1}{L} = 0.3$), and Case 3 (non-rectangular enclosure with $\frac{L_1}{L} = 0.5$), and compared with conventional rectangular enclosure of same volume of PCM respectively, when 800 W/m^2 of solar radiation is imposed on PV/PCM system.

when PV/PCM system is exposed to a solar radiation of 800 W/m^2. Some of the radiation is returned back to surroundings due to convective and radiative losses from the glass surface and the remaining is absorbed and transferred in the form of heat to PCM enclosure through glass and PV layer respectively. Therefore, melting process starts approx. 5 minutes after of incidence of solar radiation. Melting is initially dominated by conductive heat transfer. Viscous forces dominates in the fluid during this time period as melting layer thickness is very small. Solid-liquid interface remains parallel to the adjacent wall of PV panel because these viscous forces opposes the fluid flow in this mode of heat transfer. As the time progresses the melting layer thickness starts to grow and buoyancy forces becomes large enough to overcome these viscous forces. At this stage a natural convection current is initiated in the melting fluid and as a consequence, erosion of solid-liquid interface is observed at the top part of melting region. This erosion is clearly observed at 30 minutes although natural convection starts to dominate at approximately 15 minutes. The development of buoyant force encourages the circulation current in the top part of enclosure creating a concave curvature on the top of melt front while in the rest of cavity melt front is almost linear and the tilt increases with time. The melting front remains concave in the top region of enclosure till it reaches opposite wall, after reaching the right wall the curvature of melting front changes from concave to convex as shown in Figure 2.5(a) at approximately 60 minutes. At this stage of melting top part of enclosure liquid gets heated due to convective heat transfer and temperature of PCM increases and melting the lower part of PCM slows down. Since convective heat transfer is dominated in the top part of enclosure, it is desirable that suitable volume of PCM must be strategically placed in the top part of cavity.

Figure 2.5(b), 2.6(b) and 2.7(b) depicts the melting process of PCM in a non-rectangular enclosure (type – B) for case 1, case 2 and case 3 respectively. Melting behavior in non-rectangular enclosure is same as that of rectangular enclosure, however, melting rates are observed to be different due to asymmetric distribution of PCM. This non-rectangular enclosure has the same volume of PCM as of rectangular one but bifurcation mass ratio is greater than 1. The bifurcation mass ratio is 2.63, 2.07 and 1.67 for non-rectangular enclosure (type – B) for case 1, case

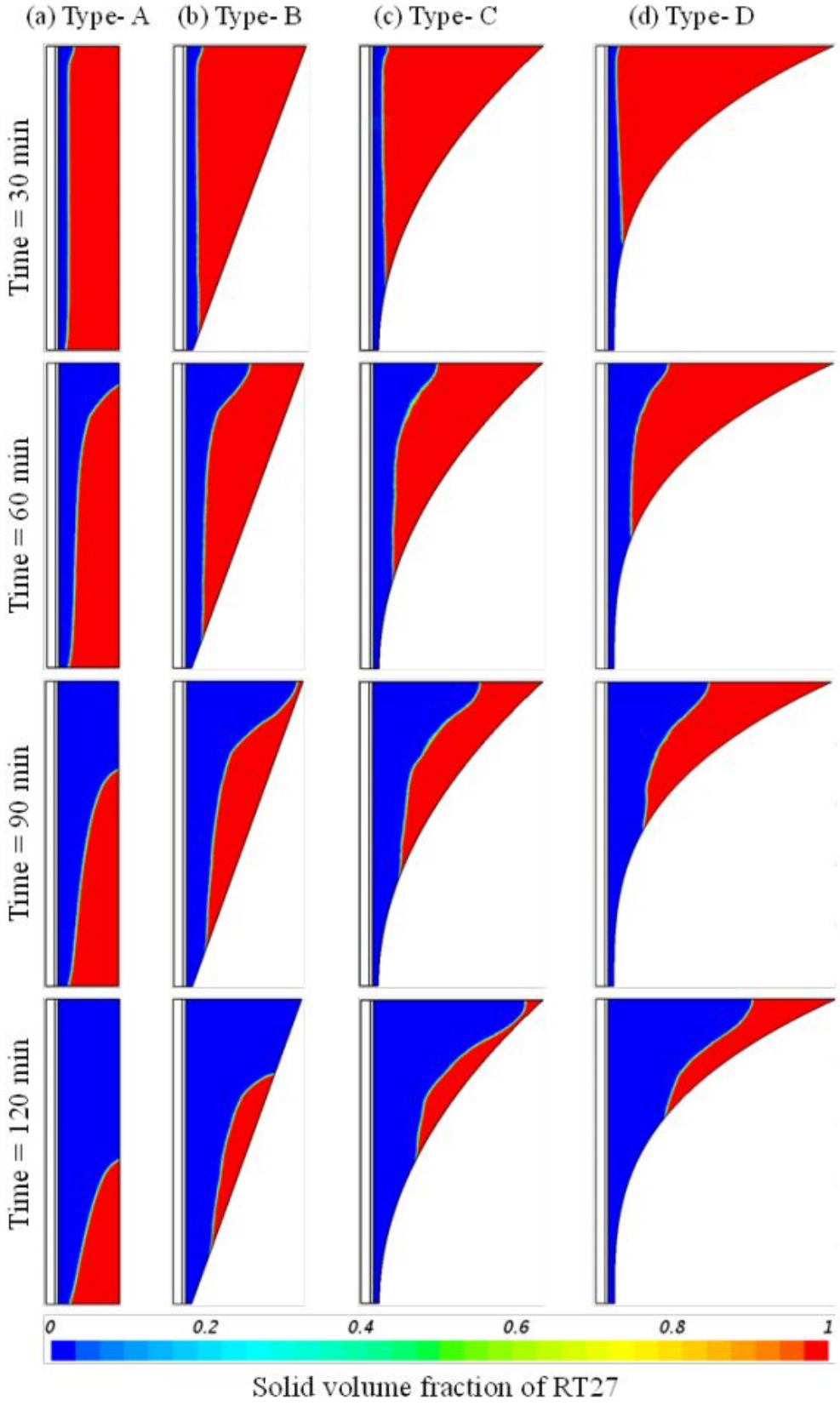

Figure 2.5: Sequential solid fraction contours of the melting process of PCM in rectangular enclosure (type – A) and in non-rectangular enclosure (type – B, C, and D) for Case 1.

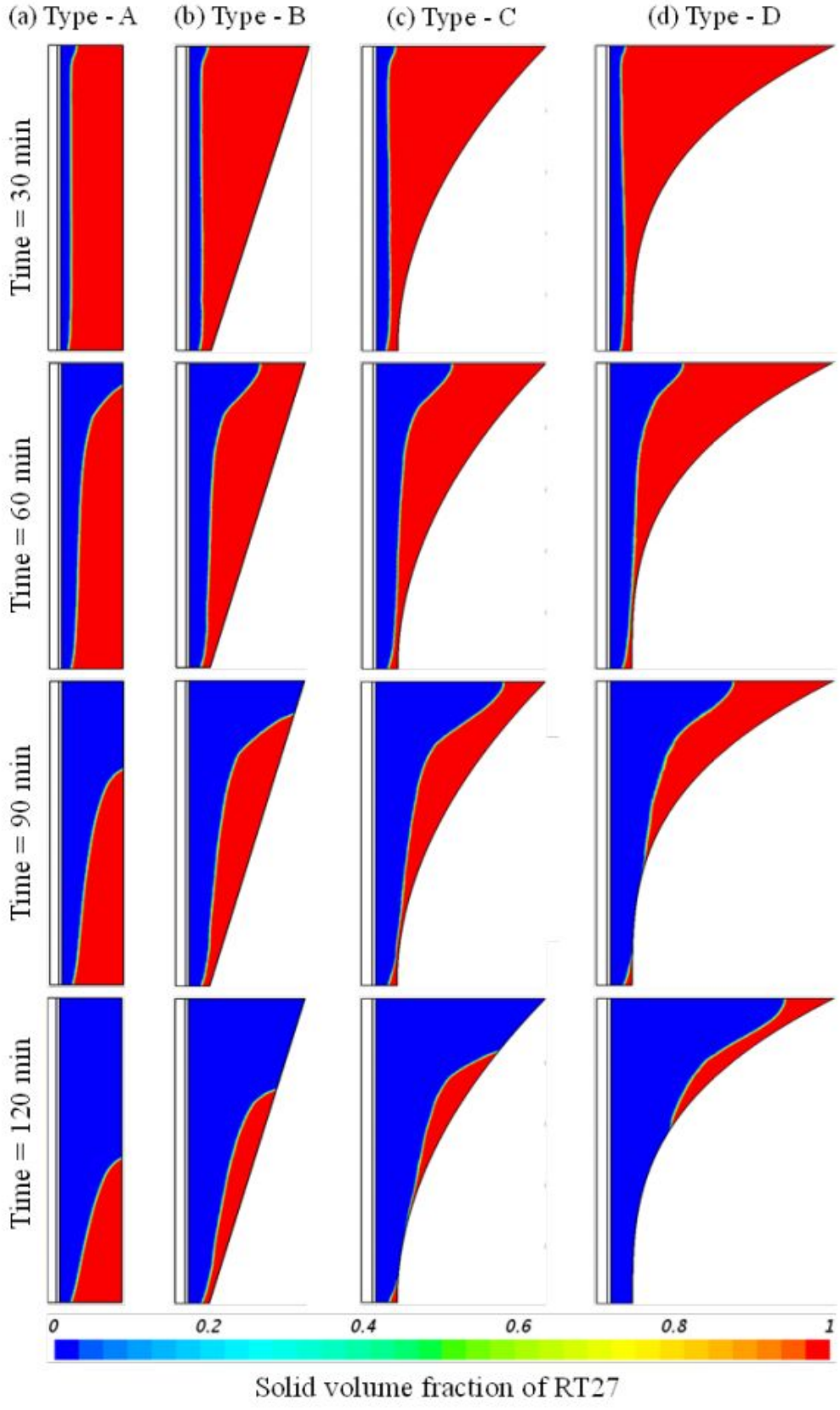

Figure 2.6: Sequential solid fraction contours of the melting process of PCM in rectangular enclosure (type – A) and in non-rectangular enclosure (type – B, C, and D) for Case 2.

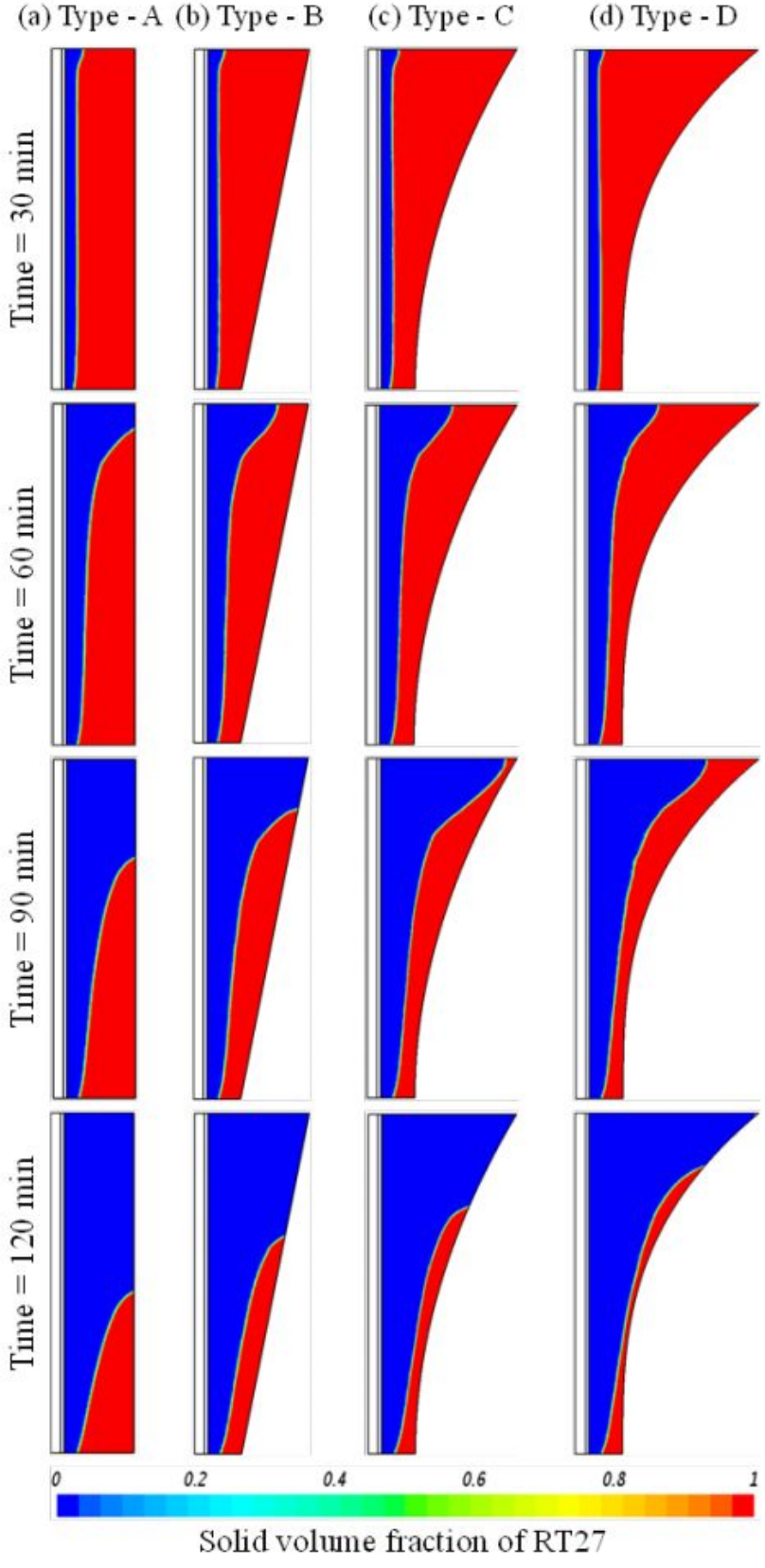

Figure 2.7: Sequential solid fraction contours of the melting process of PCM in rectangular enclosure (type – A) and in non-rectangular enclosure (type – B, C, and D) for Case 2.

2 and case 3 respectively while for rectangular enclosure, the ratio is 1.These higher mass ratio clearly indicates that more amount of PCM is available for natural convection dominated melting that delays the time duration of melting front reaching the right wall. The time period of melting front reaching the right wall is 92 minutes for case 1, 84 minutes for case 2 and 76 minutes for case 3 respectively for non-rectangular enclosure (type – B) while for rectangular enclosure it is only 56 minutes. In other words, maximum delay in quasi-steady regime is about 64% higher than conventional design, which is reasonably significant. Increase in this time period increases the quasi-steady convective heat transfer to dominate more and thus increasing the melting rate. Due to longer quasi-steady regime case 1 has highest melting rate and then melting is slow down as duration of quasi-steady regime decreases.

Further, the non-rectangular enclosure is modified by changing the profile of the right wall of the enclosure, in type – B the profile of right wall was linear that changes to parabolic in type – C and cubic in type – D. Changing of profiles causes efficient distribution of PCM in enclosure and redistributing more PCM in the top side of enclosure where convective heat transfer is more dominant. The melting process of PCM in a non-rectangular enclosure (type – C) for case 1, case 2 and case 3 are shown in Figure 2.5(c), 2.6(c) and 2.7(c) respectively while for non-rectangular enclosure (type – D) for case 1, case 2 and case 3 are shown in Figure 2.5(d), 2.6(d) and 2.7(d) respectively. The bifurcation mass ratio is 5.15, 3.21 and 2.20 for non-rectangular enclosure (type – C) for case 1, case 2 and case 3 respectively and 8.41, 4.16 and 2.55 for non-rectangular enclosure (type – D) for case 1, case 2 and case 3 respectively. The quasi-steady regime of melting duration is protracted significantly for type – C enclosure in case 1 as melting front doesn't reaches the right wall but for case 2 and case 3 it exists upto 116 minutes and 94 minutes respectively. The melting rate is lower in case 1 as compare to case 2 and case 3 despite having longest quasi-steady regime, this is due to a very high mass ratio i.e very less amount of PCM in the lower side of enclosure. The physical interpretation of this observation is very high mass ratio degrades the heat transfer despite convective heat transfer being dominant in the region but strength of convection current weakens due to very less amount of PCM in the bottom. For type – D enclosure the quasi-steady regime in case 1 and case 2 never ends during the simulation of 120 minutes and melting front never reaches the right wall while for case 3 it ends upto 117 minutes. Melting rate is lower in case 1 and case 2 due to higher bifurcation mass ratio but for case 3 it is higher due to optimum mass ratio and long lasting quasi-steady regime.

Visual observations clearly reveal that in non-rectangular enclosures (all types), large volume of PCM is available for natural convection dominated melting regime but at the same time there must be sufficient amount of PCM in the bottom side of enclosure to produce enough convection current. So an optimum bifurcation mass ratio with best fitted profile of right wall is required.

2.3.2 Temperature distributions

Temperature distributions inside the PCM enclosure and PV cell for all different type of configurations is shown in Figure 2.8. In rectangular enclosure (type – A) temperature in the top side of enclosure is 46.72°C while in the lower side temperature is very close to 29.8°C. This is due to the fact that melting is dominated by natural convection and faster melting is observed in the top side due to formation of circular currents. So temperature of liquid PCM starts to increase due to sensible heating in the later stages of melting as shown in Figure 2.8(a). As a result of this rise in temperature of PCM the temperature of PV cell also rises in the similar pattern and affect the performance of PV/PCM system adversely.

Figure 2.8(b) depicts the temperature distributions inside PCM enclosure PV cell for case 1, case 2 and case 3 respectively in type – B configuration. Temperature in the top side of enclosure dropped significantly as compare to type – A configuration while in the bottom side of enclosure temperature is increased marginally. Melting of PCM is also increased in lower side of enclosure due lower value of $\frac{L_1}{L}$ in case 1. Hence, there is marginal sensible heating of liquid PCM in the lower side which increases the temperature of PCM to 30.5°C in lower side but the temperature in upper side decreases to 38.6°C. In overall scenario temperature is 11.26% lower than type – A configuration. As the ratio $\frac{L_1}{L}$ increases the amount of PCM in the bottom side of enclosure increases and in the top side decreases, and hence, temperature in the bottom side decreases and in top side increases in case 2 and case 3. There is increment of 2.23% and 4.66% in average PCM temperature for case 2 and case 3 as compare to case 1. This is due to convection dominated melting and sensible heating of liquid PCM. The effect of temperature distribution in PCM enclosure is also seen on PV cell and similar temperature distribution is seen.

Changing the profile of right wall of non-rectangular enclosure from linear to parabolic and cubic in type – C and type – D respectively decreases the amount of PCM in the bottom side and increases in top side of enclosure. Due to this arrangement of PCM temperature in the top side of enclosure dropped to 34.5°C for type – C and 33.8°C for type – D configuration but in the bottom side increases dropped to 41°C for type – C and 46.78°C for type – D configuration in case 1 as shown in Figure 2.8(c-d). The average temperature drop is 16.07% and 16.15% in type – C and type – D respectively as compare to type – A configuration. In case 2 and case 3 for a greater value of $\frac{L_1}{L}$ more uniform temperature distribution is seen and temperature distribution is similar to all other enclosure (higher in top side and lower in bottom side. The average temperature rise is 2.73% in case 2 and 7.26% in case 3 for type – C configuration as compare to case 1. Type – D configuration has more uniform distribution of temperature inside enclosure as compare to all other configuration in case 2 and case 3. The average temperature rise is also marginal 0.9% in case 2 and 1.26% in case 3 when compared to case 1. This is due to PCM is perfectly distributed for natural convection driven melting and more heat gain is in form of latent heat as compare to other configurations.

Figure 2.9 shows the variation of temperature along the height of PV panel at 120 minutes for case 3. PV cell temperature attains a high but uniform value (56.78°C) when no PCM enclosure is attached to PV panel. Attachment of rectangular PCM enclosure decreases the PV cell temperature but uniformity along the height of PV panel is lost. This is due to thermal stratification in top part of PCM enclosure. PV panel attains a value of 47.58°C at the top end while at the bottom end temperature is only 30°C. This significant difference in temperature at both ends can be minimized by using non-rectangular PCM enclosure. Type – D non-rectangular enclosure decreases the top end temperature to 36.9°C while the bottom end is still at 30°C. Hence a more uniform distribution along the height of PV panel is obtained in Type – D configuration. This uniform distribution of temperature is necessary for uniform efficiency and power generation in PV panel.

2.3.3 Effect of enclosure design on flow behavior during PCM melting

To get a deeper insight of melting process we need to understand the flow behavior of the liquid PCM inside the enclosure under the effect of natural convection (see Figure 2.10). After the convection regime, liquid starts to ascend along the heated wall and reaches the top region of enclosure. This movement transfers more heat and the cooled liquid PCM descends downwards along the solid-liquid interface. This leads to the formation of clockwise circular flow patterns within the enclosure that are induced by buoyancy forces. Heated liquid PCM cause more melting in the top region of enclosure due to these circular flow patterns. When melting front reaches the right wall the solid starts to shrink down in the enclosure and secondary clockwise circular flow patterns formation can be seen in the lower part of enclosure due to presence of cold unmelted solid in the bottom part of enclosure (see Figure 2.10). The melting rate decays in solid shrinking regime because primary clockwise loops that travel along the length of enclosure transfer most of heat to liquid PCM in top region and increases its sensible heating. Figure 2.10 shows the velocity field (streamlines superimposed with solid volume fraction field) for case 3 at 120 minutes for all type of enclosure configurations. In type – A rectangular enclosure the quasi-steady convection regime ends sooner than any other configuration, and hence, secondary clockwise flow patterns starts to form a bit earlier that causes the melting rate to decay. This causes the duration of solid shrinking regime to increase. This decrease in melting rate increases the average temperature of liquid PCM and as a consequence, the PV cell temperature also rises which affects its performance. In type – B non-rectangular enclosure the formation of secondary clockwise flow patterns delays due to increased upper thickness of non-rectangular enclosure. Similarly for type – C and D configuration the increased upper thickness of PCM enclosure delays the formation of secondary vortices further and increasing the melting rate. It is clear from the Figure 2.10 that the intensity of the streamlines are high in type – A and least in

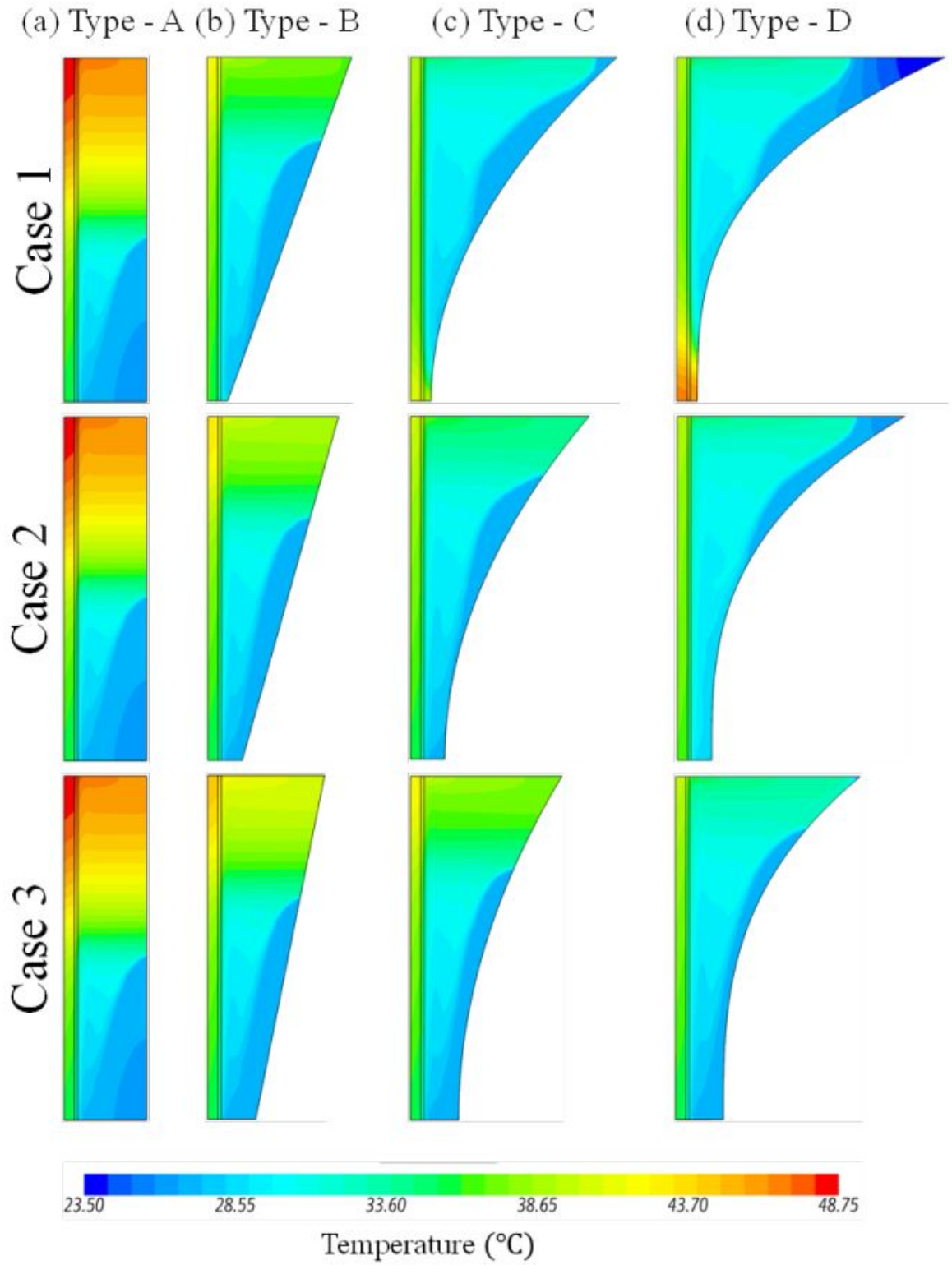

Figure 2.8: Temperature distribution in all type of configuration of PV/PCM systems at 120 minutes.

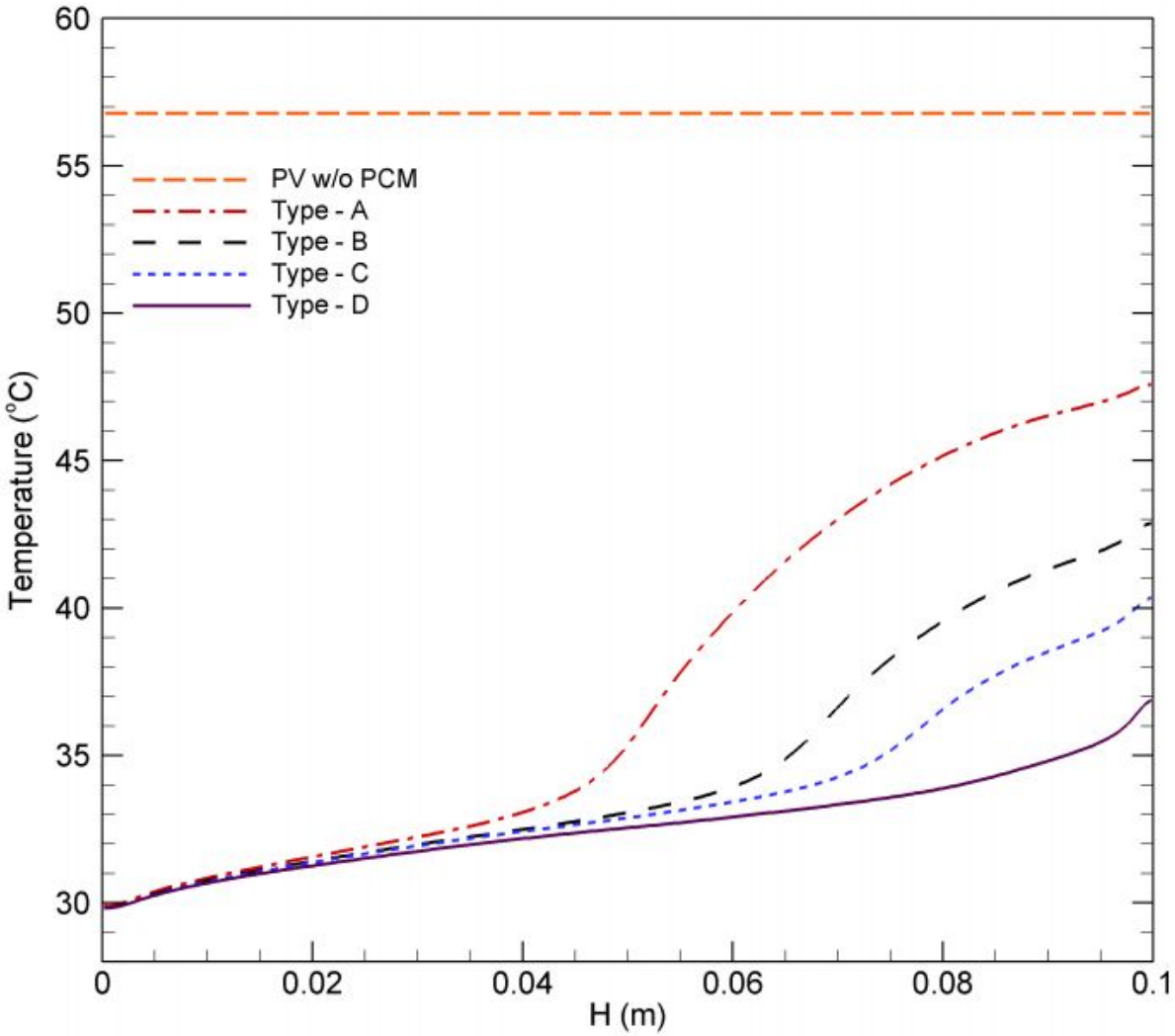

Figure 2.9: Variation of Temperature along the height of PV panel at 120 minutes for case 3.

type – D because of the delay of secondary vortices formation in type – D configuration. Thus type – D configuration shows better heat transfer performance than any other configuration.

2.3.4 Heat transfer characteristics

2.3.4.1 Melting rate

Figure 2.11 compares the liquid fraction in an enclosure for all different type of configuration for case 3 while for case 1 and case 2 is summarized in Table 2.4. For all configurations liquid fraction almost varies linearly with time. As solid PCM shrinks down in rectangular enclosure (type – A), liquid fraction deviates from the linear trend very early and melting rate decreases due to suppression of convection current while in non-rectangular enclosures (type – B, C and

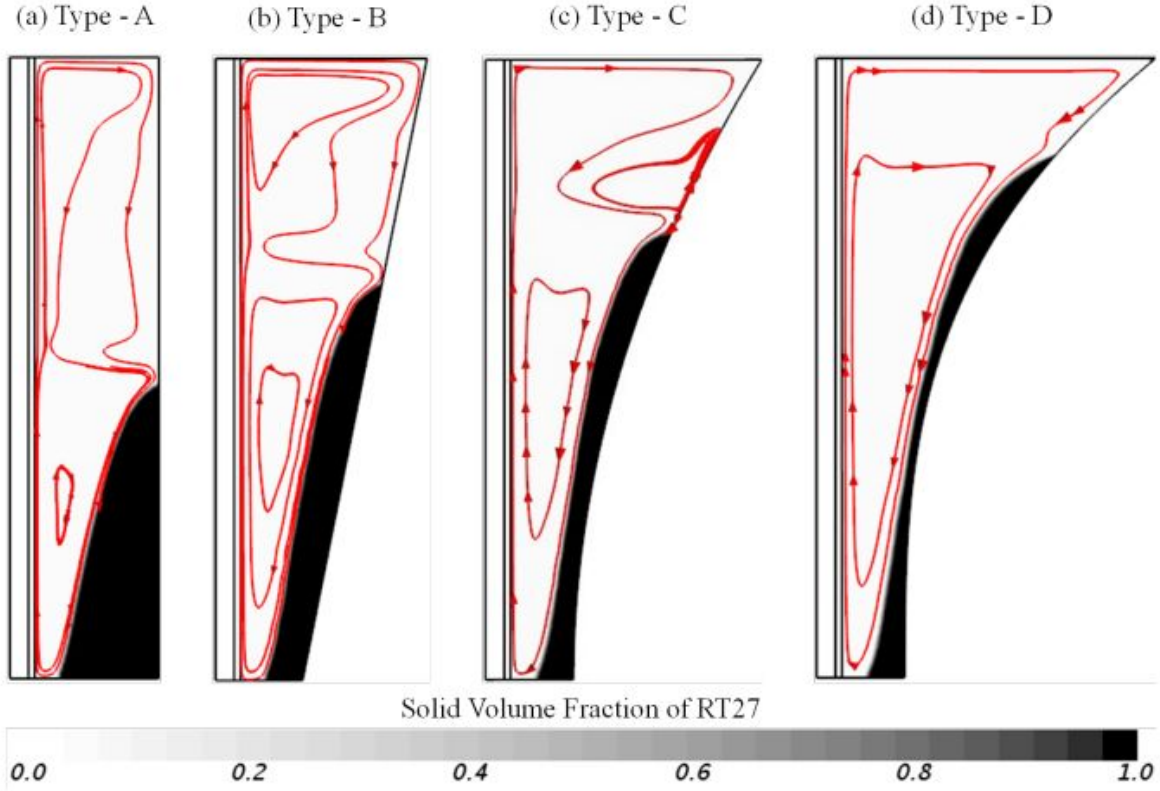

Figure 2.10: Velocity streamlines superimposed on solid volume fraction map for Case 3 at 120 minutes. Black color on the right wall shows solid PCM.

D) the liquid fraction varies linearly with time for longer durations. This means that arranging more PCM in convection dominated region of enclosure increases the melting rate significantly.

In case 1 ($\frac{L_1}{L} = 0.1$), melting in type – D configuration is lower than type – B configuration while melting in type – C configuration is comparable to type – B despite of having more PCM in top side of enclosure. The melting in type – A was 75.17% in duration of 120 minutes while in type – B and C it reached up to 84.16% and 84.56% respectively, while in type – D it is only 77.91% . There is an increase of 11.96%, 12.48% and 3.64% in melting fraction in type – B, C and D respectively as compare to type – A. type – C and D performed better but there is decrease in convective heat transfer due to low amount of PCM in bottom side. There must be higher value of $\frac{L_1}{L}$ so that amount of PCM in the bottom side of enclosure can be increased.

In case 2 ($\frac{L_1}{L} = 0.3$), maximum melting rate is observed in type – C configuration while melting in type – D configuration is also comparable to previous one. Melting in type – B configuration has been slowed down marginally as compare to case 1. By 120 minutes, 88.09% of PCM melted in type – C configuration, and 87.72% and 83.07% melting is observed in type – D and B configuration respectively. So increasing the ratio $\frac{L_1}{L}$ enhances the melting rate in the enclosure. type – C configuration shows an improvement of 17.18% as compare to typical rectangular configuration (type – A), while there is an improvement of 16.69% and 10.51% in type – D and

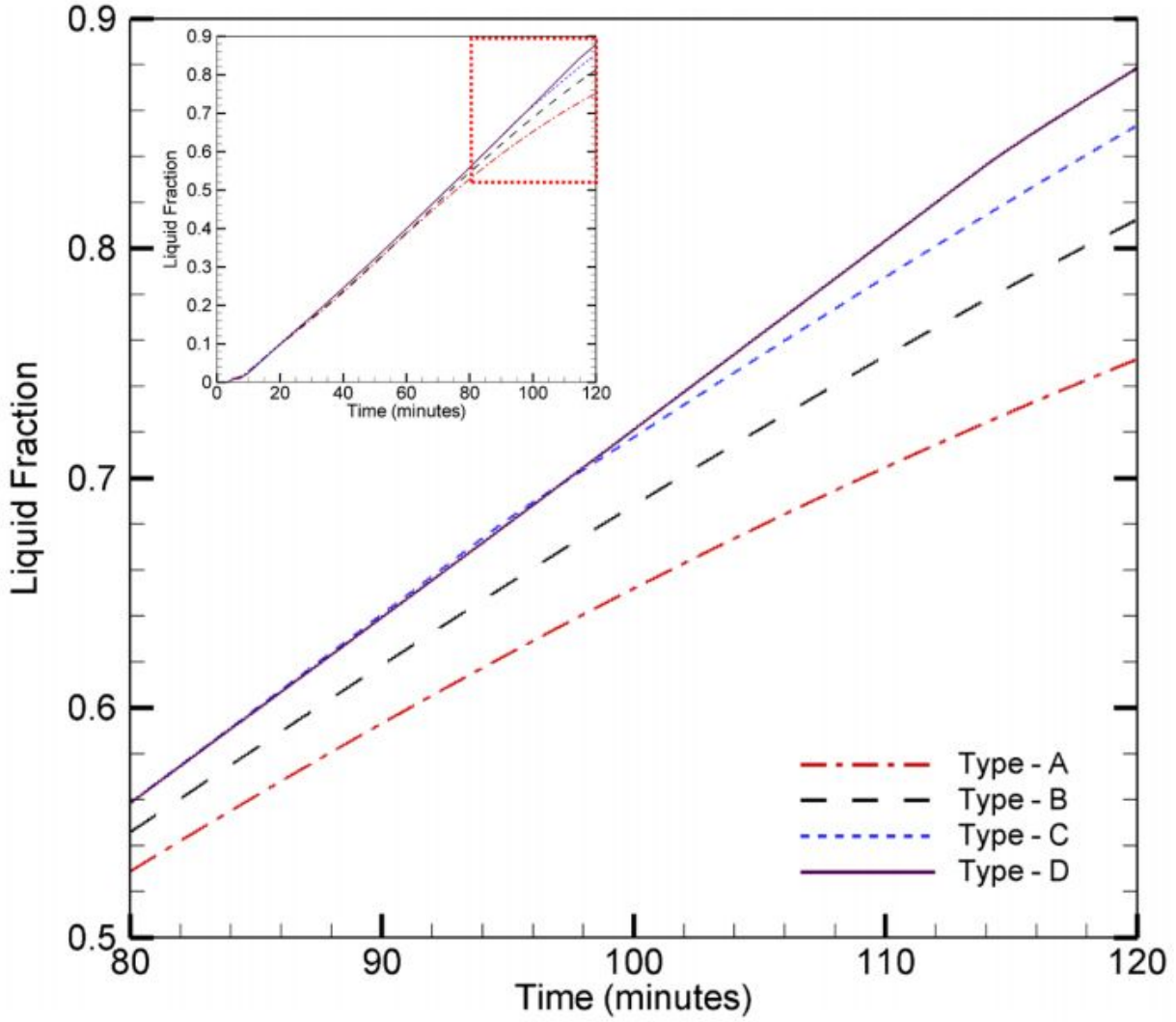

Figure 2.11: Expanded view of liquid fraction vs time shown in inset for all type of configurations for case 3.

type – B respectively. Further there are chances of improvement by increasing the value of $\frac{L_1}{L}$ in type – C and D configurations.

In case 3 ($\frac{L_1}{L} = 0.5$), melting slowed down in type – B and C configuration as amount of PCM on the top side has been decreased compared to previous cases. The liquid fraction vs time curve shrinks down in later stages of melting in type – B and C configuration while for type – D configuration it still shows linear trend as shown in Figure 2.11. It has been found that 87.84% of liquid has been changed from solid to liquid in type – D configuration which is 16.85% higher than conventional type – A configuration. A melting of 85.35% and 81.26 % in type – C and B configurations respectively was noticed, which is 13.53% and 8.09% higher than the conventional configuration.

From the above observation it can be concluded that melting rate is maximum in type – C configuration in case 2 but type – D configuration shows the comparable melting to type – C in

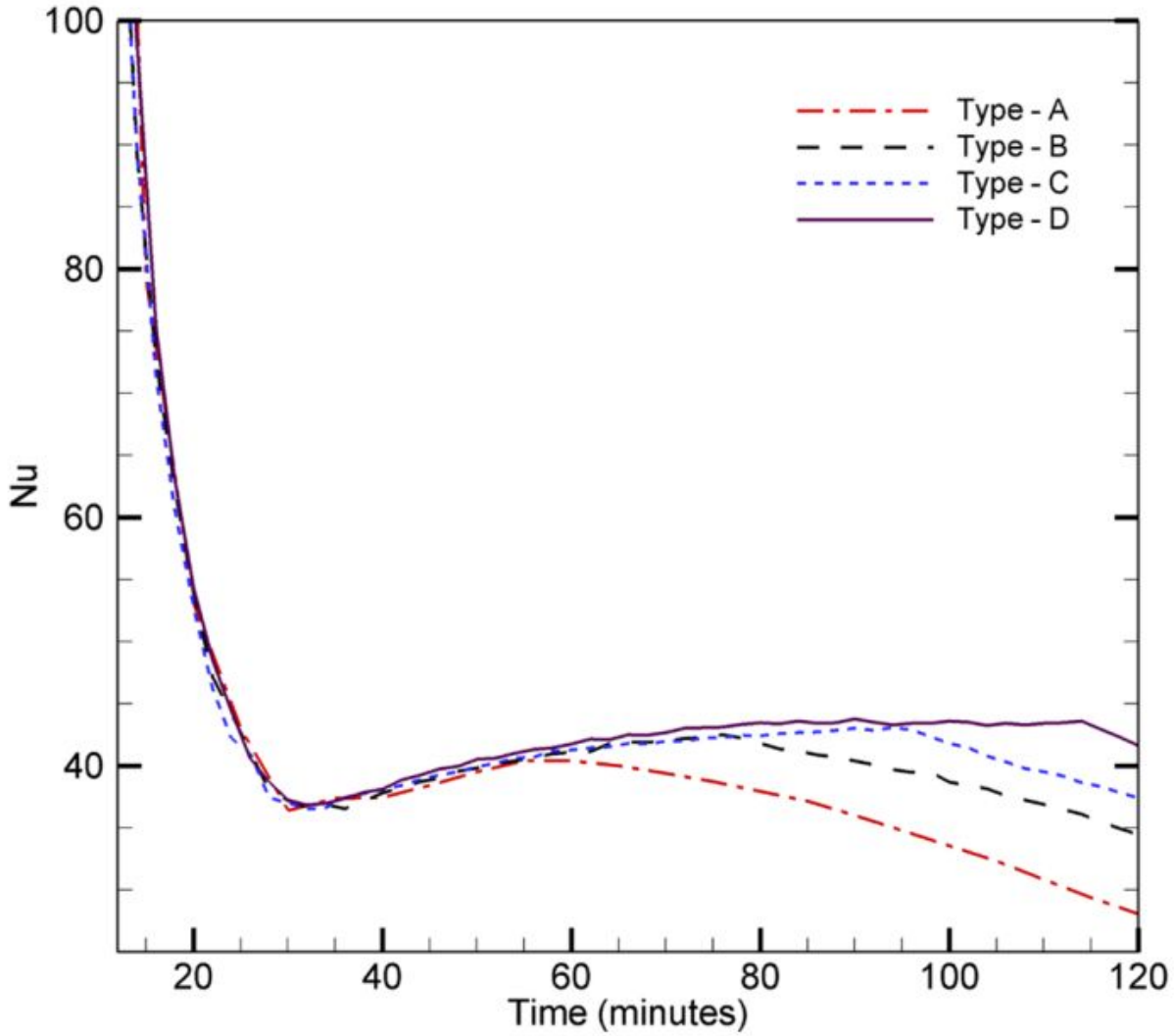

Figure 2.12: Variation of Nusselt number for all type of configuration for case 3.

case 2. It is also found that type – D configuration of case 3 also shows the comparable melting rate as for type – C configuration of case 2 but type – D configuration shows more uniform temperature distribution and as a result lower PV cell temperature than any other configuration. Hence, type – D configuration is most suitable configuration of PV/PCM system.

2.3.4.2 Nusselt number

Figure 2.12 depicts the variation of Nusselt number with time in all type of configuration for case 3 while for case 1 and case 2 is summarized in Table 2.4. The surface averaged Nusselt number (Nu) at any instant of time (t) can be defined as:

$$Nu(t) = \frac{h(t)H_{pv}}{k} \tag{2.15}$$

The characteristic length is taken to be the height of enclosure (H_{pv}) for all configurations

for the sake of comparison. Initially Nusselt number shows a very high value due to very thin fluid layer causing a low thermal resistance. Conduction regime prevails up to 15 minutes approx. for all type of configurations. As the convective currents develops over time, dominance of conductive heat transfer decreases resulting in Nusselt number to a local minimum. Mixed regime ends approximately at 30 minutes and beyond this time melting is dominated by convective heat transfer. Nusselt number starts to increase and becomes nearly constant. This quasi-steady convection regime ends as melting front reaches the right wall. Nusselt number starts to decrease linearly in this solid-shrinking regime. Longer time span of quasi-steady regime enhances the convective heat transfer and exhibits improved melting rates.

As discussed earlier in section 3.1, type – A configuration has smallest span of quasi-steady regime (upto 56 minutes) while type – D configuration (case 3) exhibit longest quasi-steady regime (upto 117 minutes). Melting front never reaches the right wall in type – C and D configuration (case 1) and type – D configuration (case 2) but still Nusselt number shows a lower value because insufficient amount of PCM in the lower part of enclosure. Type – C configuration (case 2) also exhibit quasi-steady regime upto 116 minutes. Type – D configuration performs better than all configuration and shows good heat transfer characteristics in PCM enclosure. When compared with the rectangular enclosure design, type-D enclosure enhanced the quasi-steady regime by (117-56)/56 = 109% and Nusselt number (at 120 minutes) by 48.32%. Hence, it is best design among the investigated encapsulations.

2.3.4.3 Heat storage Performance

Energy storage density (*ESD*) is defined as the possible derivable energy from the system. *ESD* increases with time due to evolution of the melting process. For a thermal energy storage system *ESD* at any time is defined as:

$$ESD = \frac{1}{V_{PCM}} \iiint_V (\rho c_p \Delta T + \rho f_l L_{sf}) dV \tag{2.16}$$

Where $\Delta T = T_{PCM} - T_i$ and T_{PCM} is local PCM temperature, T_i is the initial temperature and V_{PCM} is the total volume of PCM enclosure. This amount of ESD is required to melt f_l fraction of PCM.

Figure 2.13(a) shows the variation of *ESD* with time for different designs of PCM encapsulation. *ESD* varies linearly with time for all configuration except conventional rectangular configuration (type – A). Suppression of convection current during later stages of melting due to thermal stratification is the reason of this decrement in *ESD* in rectangular enclosure. Apart from the rectangular enclosure, the type – D enclosure in case 1 shows the worst performance. This is due to very large mass on the top side of enclosure which hinders the melting process. Figure 2.13(b) represents the all three i.e. sensible, latent and total energy storage density for

Table 2.4: Results of PV and PV/PCM systems. The results in bold are crucial for comparing some of the top performing configurations to conventional ones.

Variable	Case	Type/ Time	0	15	30	60	90	120
		w/o PCM	**20**	**56.74**	**56.75**	**56.78**	**56.78**	**56.78**
T_{pv}(°C)		A	**20**	**32.12**	**34.86**	**34.84**	**36.21**	**39.28**
		B	20	32.22	34.93	34.83	34.67	35.57
	Case1	C	20	32.29	35.79	35.46	35.52	35.75
		D	20	32.57	37.19	36.97	37.05	37.38
		B	20	32.2	34.93	34.8	34.74	35.99
	Case2	C	**20**	**32.49**	**35.06**	**34.75**	**34.62**	**34.97**
		D	20	32.15	34.88	34.63	34.56	35.22
		B	20	32.09	34.88	34.81	34.99	36.65
	Case3	C	20	32.15	34.97	34.77	34.61	35.72
		D	**20**	**32.02**	**34.88**	**34.71**	**34.52**	**34.76**
		w/o PCM	**12.64**	**10.85**	**10.84**	**10.84**	**10.84**	**10.84**
η_{pv}(%)		A	**12.64**	**12.05**	**11.91**	**11.91**	**11.84**	**11.69**
		B	12.64	12.04	11.91	11.91	11.92	11.87
	Case1	C	12.64	12.04	11.87	11.88	11.88	11.87
		D	12.64	12.03	11.8	11.81	11.81	11.79
		B	12.64	12.04	11.91	11.92	11.92	11.86
	Case2	C	**12.64**	**12.03**	**11.9**	**11.92**	**11.93**	**11.91**
		D	12.64	12.04	11.91	11.92	11.93	11.9
		B	12.64	12.05	11.91	11.92	11.91	11.83
	Case3	C	12.64	12.05	11.91	11.92	11.93	11.87
		D	**12.64**	**12.05**	**11.91**	**11.92**	**11.93**	**11.92**
		A	**0**	**0.063**	**0.164**	**0.387**	**0.593**	**0.751**
f_l		B	0	0.067	0.172	0.392	0.629	0.842
	Case1	C	0	0.069	0.172	0.39	0.615	0.845
		D	0	0.066	0.162	0.365	0.573	0.779
		B	0	0.066	0.17	0.391	0.627	0.831
	Case2	C	**0**	**0.075**	**0.183**	**0.41**	**0.647**	**0.881**
		D	0	0.067	0.179	0.408	0.645	0.877
		B	0	0.063	0.166	0.389	0.619	0.813
	Case3	C	0	0.064	0.172	0.399	0.641	0.853
		D	**0**	**0.061**	**0.171**	**0.399**	**0.639**	**0.878**
		A	**-**	**79.17**	**36.38**	**40.35**	**35.97**	**28.04**
Nu		B	-	76.96	36.48	40.59	41.85	36.01
	Case1	C	-	76.57	30.44	34.73	34.13	32.44
		D	-	99.76	26.92	29.86	29.28	27.18
		B	-	72.26	36.6	41.58	41.91	36.61
	Case2	C	**-**	**72.04**	**36.54**	**41.29**	**42.95**	**39.89**
		D	-	84.75	37.76	42.56	42.47	34.99
		B	-	81.13	37.18	41.07	40.37	34.47
	Case3	C	-	80.7	36.99	41.27	43.03	37.38
		D	-	**86.97**	**37.2**	**41.73**	**43.77**	**41.59**

various design configurations. It can be seen that sensible *ESD* is maximum for type – A configuration due to thermal stratification. In all modified configuration sensible *ESD* decreases and latent *ESD* increases due to increment of convection regime.

In each configuration sensible *ESD* decreases by increasing lower thickness ratio ($\frac{L_1}{L}$) from case 1 to case 3. Latent *ESD* get maximized only at optimum value of lower thickness ratio i.e $\frac{L_1}{L} = 0.1$ for type – B enclosure, $\frac{L_1}{L} = 0.3$ for type – C enclosure and $\frac{L_1}{L} = 0.5$ for type – D enclosure. Total *ESD* is the sum of both sensible and latent *ESD*. Total *ESD* is maximum for type – C enclosure at $\frac{L_1}{L} = 0.3$ (case 2) in all of cases while type – D enclosure at $\frac{L_1}{L} = 0.5$ (case 3) has value significantly closer to maximum case. Type – C enclosure at $\frac{L_1}{L} = 0.3$ has best heat storage performance.

2.3.5 Performance characteristics

2.3.5.1 PV cell temperature

Figure 2.14 shows the variation of surface averaged PV cell Temperature with time in all four type of configuration for case 3 while for case 1 and case 2 is summarized in Table 2.4. PV cell temperature bears direct signature of PCM melting processes as discussed above. For solar radiation of 800 W/m^2, temperature of PV cell rises quickly and reaches to 56.78°C when no PCM enclosure is attached to the PV panel. Attaching a PCM enclosure decreases the PV cell temperature as PCM absorbs heat as latent heat at constant temperature.

The PCM enclosure works as latent heat storage device. In type-A configuration temperature rises quickly and then become constant at 34.7°C as PCM starts to absorb heat at constant temperature. Thus PV/PCM system works at constant and low temperature until the PCM in the upper region of the enclosure melts or melting front reaches the right wall. After the melting front reaches the right wall PV cell temperature begins to rise and reaches to 39.28°C at the end of 120 minutes, which is still 30.82% lesser comparatively when no PCM is attached.

In case 1, type – B configuration works on constant temperature for longer time due to longer quasi regime of melting and PV cell temperature reaches to 35.57 °C at end of 120 minutes which is 37.35 % lower than the configuration without PCM and 9.44 % lower than the type-A configuration. PV cell temperature drops down to 35.75 °C for type – C configuration which is 37.04% lower than configuration without PCM and 37.37 °C for type – D configuration which is 34.17% lower than no PCM enclosure configuration.

In case 2, PV cell temperature is reduced to 35.98 °C in duration of 120 minutes which is 36.62 % lesser than system having no PCM enclosure. For type – C and D PV cell temperature goes up to 34.97°C and 35.21 °C respectively. There is a decrease of 38.41% and 37.98% in PV cell temperature for type – C and D respectively as compare to PV panel without PCM enclosure. For type – B PV cell temperature decreases up to 36.64°C and for type – C and D PV cell temperature goes up to 35.72°C and 34.76 °C respectively. There is a decrease of 35.45%, 37.08% and 38.77%

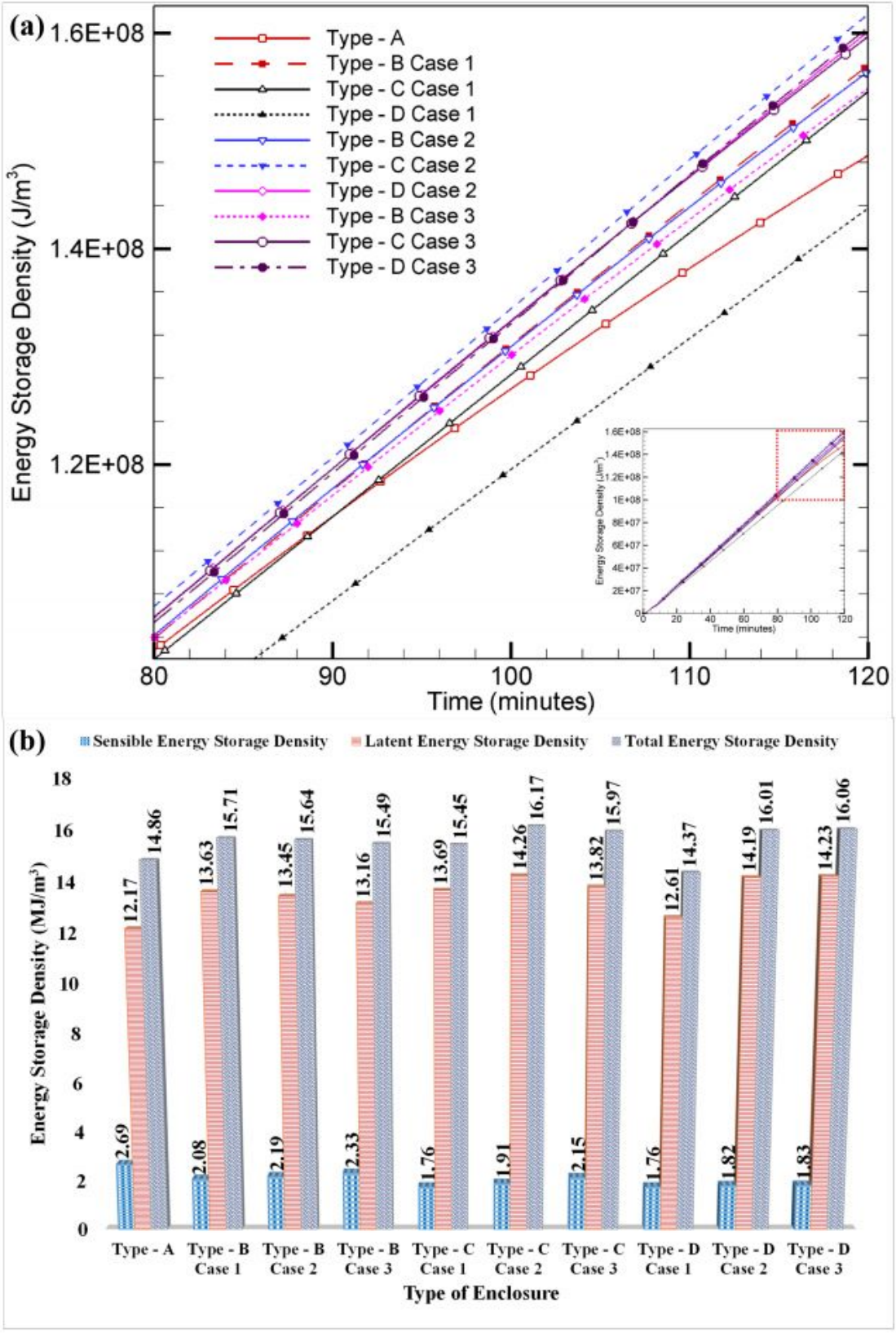

Figure 2.13: (a) Expanded view of variation of ESD with time shown in inset, (b) ESD values for all configurations at 120 minutes.

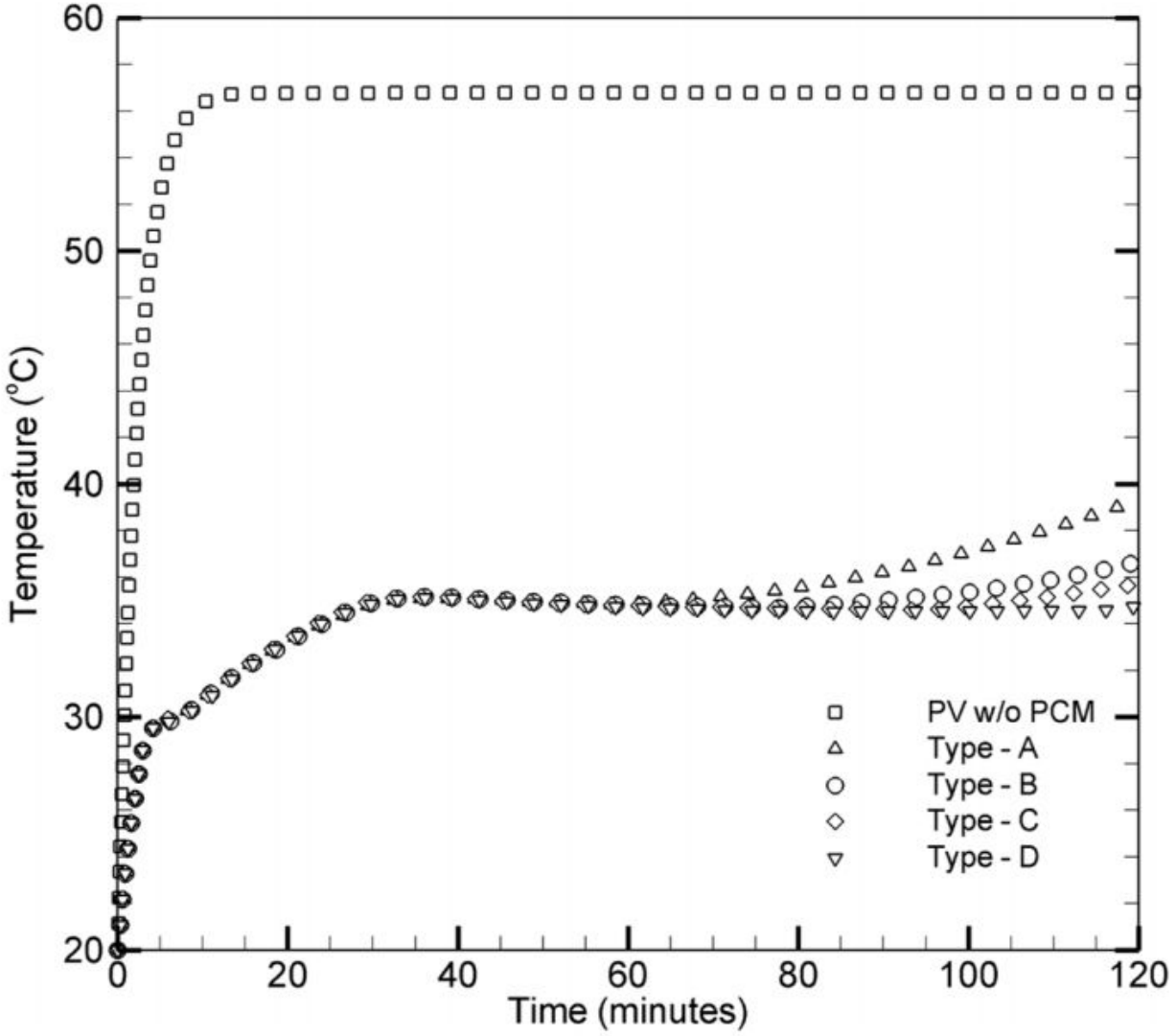

Figure 2.14: Variation of PV cell temperature with time for all type of configuration of PV/PCM system for case 3.

in PV cell temperature for type-A, B, C and D respectively as compare to PV panel without PCM enclosure.

It has been noticed that type – D i.e. non-linear cubic profile configuration of PV/PCM system of case 3 has performed better than all other configuration with lowest PV cell temperature. This is due to more uniform distribution of temperature in the current configuration.

2.3.5.2 Effect of enclosure design on PV electrical efficiency

Lower the PV cell temperature higher would be the PV cell electrical efficiency. Variation of electrical efficiency with PV cell temperature is given in Eq. 2.14. PV panel works more efficiently at its reference temperature or any temperature below it. Hence PCM enclosures are attached to PV panel to keep its temperature close to reference value. Further, rectangular PCM enclo-

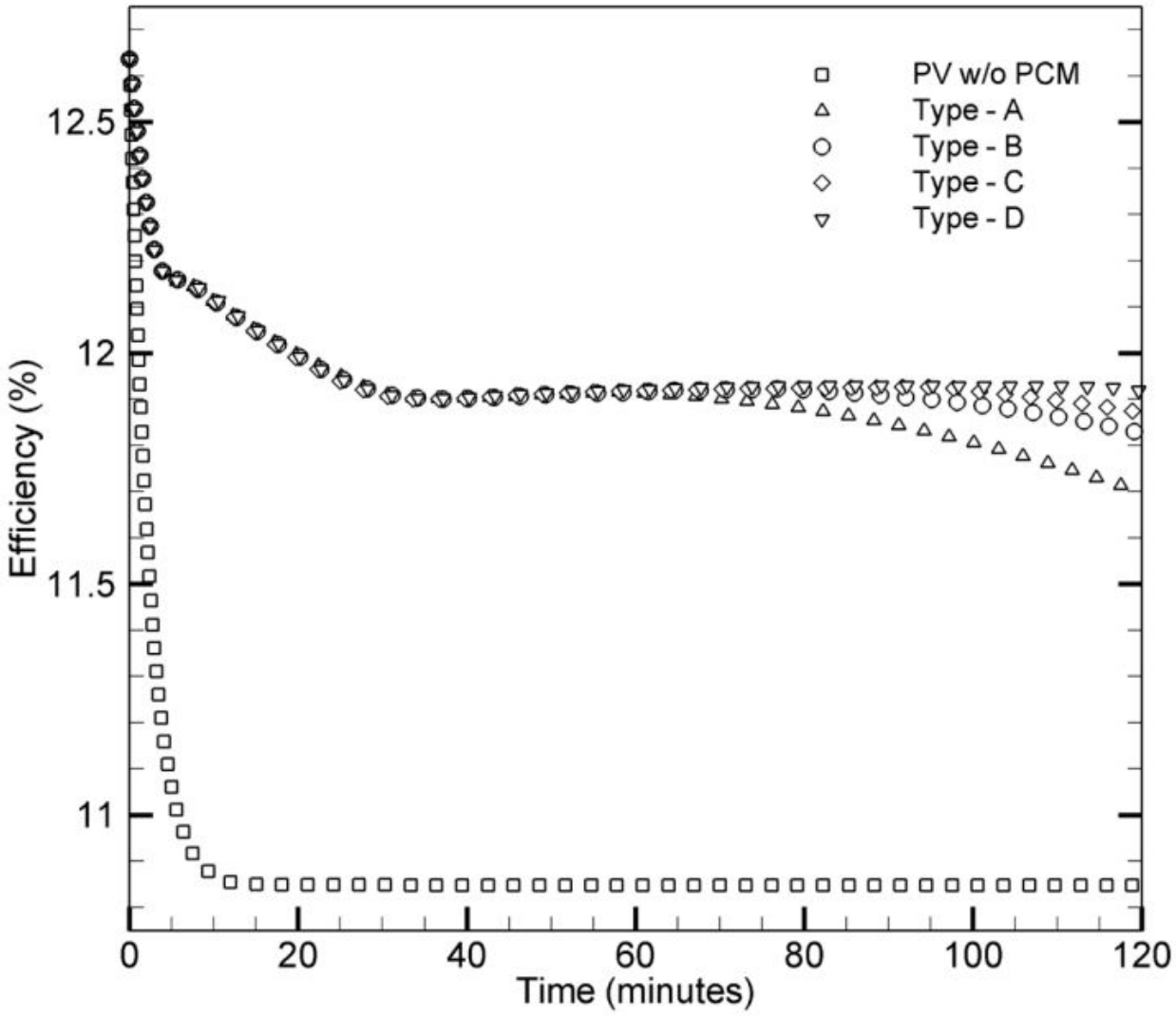

Figure 2.15: Variation of electrical efficiency with time for all type of configuration of PV/PCM system for case 3.

sure exhibit non-uniform power generation along the height as it has non- uniform temperature distribution (see Figure 2.9). Electrical efficiency decrease by up to 11.25% at top end as temperature is reported 46.58°C while at bottom it is 12.15% due to a lower temperature. A uniform temperature distribution in Type-D configuration maintains a uniform power generation and electrical efficiency. The efficiency at top increases to 11.85% while 12.15% is still maintained at bottom end. Since electrical efficiency varies along the height of PV panel due to local temperature variations, we report the surface averaged electrical efficiency on various enclosure designs. Figure 2.15 shows the variation of PV electrical efficiency with time in all the four types of configurations for case 3 while for case 1 and case 2 is summarized in Table 2.4. PV cell efficiency is 10.84% at a temperature of 56.78°C when PV is exposed to a constant solar radiation of 800 W/m^2. Putting a rectangular PCM enclosure (type-A) on the back plane of PV panel reduces the PV cell temperature to 34.7°C till the end of quasi-steady regime and as a consequence

increasing the efficiency up to 11.91%. In solid shrinking regime PCM gets overheated in top region of enclosure due to sensible heat gain of liquid PCM. This overheating of PCM increase the temperature of PV cell to 39.28°C by 120 minutes which decreases its electrical efficiency to 11.69%. Replacing the rectangular enclosure with non-rectangular enclosure of same volume, increases the time period of quasi-steady convective heat transfer process. Longer quasi-steady regime delays the melting front reaches the right wall, as a result PV panel works on constant temperature for longer time and giving better performance.

In case 1, for type – B configuration PV cell efficiency goes up to 11.88% as its temperature is 35.57°C at the end of 120 minutes. There is an increment of 7.84 % and 9.51% in efficiency of PV cell in type – A and type – B configuration respectively when compared to PV panel without any PCM enclosure. The electrical efficiency goes up to 11.87 % and 11.79% for type – C and D configuration respectively. It has been seen that electrical efficiency increased by 9.42% and 8.69 % for type – C and D respectively. The performance of type – B and C configuration are quite comparable to each other but type – B performs a little bit better in this case.

In case 2, the performance of type – B has dropped a little bit and electrical efficiency goes to 11.85 % while the performance of type – C and D has been improved as compare to previous case and efficiency goes up to 11.91% and 11.89% respectively. In this case type – C and D shows comparable performance but type – C shows a little better performance due to better arrangement of PCM. There is an increment of 9.32%, 9.77% and 9.66% in PV cell efficiency for type-A, B, C and D respectively as compare to PV panel without PCM enclosure.

In case 3, on increasing the value of $\frac{L_1}{L}$, the performance of type – B and type – C has been dropped marginally and electrical efficiency goes to 11.82% and 11.87% respectively, while the performance of the type – D configuration has been improved and electrical efficiency goes up to 11.92%. There is an increment of 9.02%, 9.43% and 9.86% in PV cell efficiency for type-A, B, C and D respectively as compare to PV panel without PCM enclosure.

Electrical performance of type – D configuration is much better than any other configuration in all cases that we have studied. It has been observed that electrical efficiency has been increased by 0.45% at every degree temperature drop.

2.4 Conclusions

In this chapter, efficiency improvement techniques of a PV panel in conventional rectangular design of PCM enclosure has been proposed using an experimentally validated numerical model. Melting rate characterization and PV panel efficiency was reported under constant boundary condition. Mass of PCM in the new encapsulation designs was strategically distributed for better thermal management by varying the profile of right wall to linear, parabolic and cubic shape with different lower thickness ratio keeping the volume of PCM same for all designs. Following are some important findings:

1. Due to suppression of convection current (smaller quasi-steady convection regime; only upto 56 minutes) in conventional rectangular enclosure, the liquid fraction deviates from the linear trend in melting – time curve. However, with strategic distribution of PCM by using non-rectangular enclosure, extends quasi-steady regime by 109% (upto 117 minutes) for cubic configuration. As a consequence Nusselt number is increased by 48% and 17% increase in melting rate was observed. Thus liquid fraction varies linearly with time for a longer time.

2. With no PCM the PV cell electrical efficiency drops to 10.84% as PV cell temperature increases upto 56.78°C. On attachment of conventional rectangular encapsulation, electrical efficiency increases to 11.69 % with an improvement of 7.84 % as PV temperature dropped to 39.28°C. However, further improvement of 1.87% in electrical efficiency was observed in cubic configuration and electrical efficiency reached to 11.92%. This is due to further decrement of 11.5% in PV cell temperature. It has been observed that electrical efficiency improved by approximately 0.45% per degree temperature rise.

3. Parabolic enclosure at $\frac{L_1}{L} = 0.3$ has best heat storage performance while cubic enclosure at $\frac{L_1}{L} = 0.5$ show better temperature uniformity among all configurations. Since thermoelectric performances are comparable in both the configurations, parabolic enclosure is recommended due to its compact design.

We hope that findings of this research would be useful to the scientific community in designing efficient PV panels integrated with non-rectangular encapsulation designs. The overall energy demand can be reduced through efficient and passive thermal regulation using better PCM encapsulation designs. It would be interesting to investigate the solidification process in the proposed designs.